

Research paper

Diagenesis of tight sandstone reservoirs in the Upper Triassic Yanchang Formation, southwestern Ordos Basin, China

Kelai Xi^{a,*}, Yingchang Cao^{a,b}, Keyu Liu^{a,b}, Songtao Wu^c, Guanghui Yuan^a, Rukai Zhu^c, Muhammad Kashif^a, Yiwei Zhao^a^a School of Geosciences, China University of Petroleum, Qingdao, Shandong, 266580, China^b Laboratory for Marine Mineral Resources, Qingdao National Laboratory for Marine Science and Technology, Qingdao, 266071, China^c Research Institute of Petroleum Exploration & Development, Beijing, 100083, China

ARTICLE INFO

Keywords:

Tight sandstone reservoirs
Diagenesis
Closed geochemical system
Yanchang Formation
Ordos Basin

ABSTRACT

In order to better predict the petrophysical properties of the tight sandstone reservoirs in the Upper Triassic Yanchang Formation, Ordos Basin, China, the nature of the diagenetic system involved was investigated using a suite of petrographic and geochemical techniques including thin section and X-Ray Diffraction analysis, scanning electron microscopy, MAPS mineralogy, Cathodeluminescence, electron probe microanalysis and fluid inclusion analysis on a set of selected tight sandstone samples. The sandstones investigated are texturally mature but compositionally immature with an average framework grain composition of $Q_{32}F_{41}L_{27}$. Authigenic quartz, calcite, and chlorite coatings are the major cements, while feldspars are partially dissolved. Two groups of quartz cement are present in the tight sandstone reservoirs. Smectite to illite conversion provided silica source for the first group of quartz overgrowth (Qo-I), while the silica source for the second quartz overgrowth (Qo-II) was mainly originated from feldspar dissolution. Calcite cements consist of two types, namely Ca-I and Ca-II. The Ca-I calcite cement contains no chlorite coatings and have higher concentrations of Fe^{2+} and Mg^{2+} , whereas the Ca-II calcite cement developed over the chlorite coatings. Plagioclase dissolution appears to be always accompanied by calcite cementation, while K-feldspar albitization forms euhedral albite locally. The burial diagenesis processes were, in most cases, not episodic but occurred as slow adjustments in response to increased burial depths and temperatures. In all the studied diagenetic minerals, elemental distributions appear to be strictly constrained by the interaction of authigenic minerals involved, indicating that the chemical reactions during the diagenesis comply well with the general principle of mass balance. The diagenesis in the Upper Triassic Yanchang Formation tight sandstones was thus mainly developed in a closed geochemical system, where mineral dissolution and precipitation are approximately balanced, and diagenetic fluids were not affected by external sources significantly. Mechanical compaction has played a more important role in destroying the primary porosities of the Upper Triassic Yanchang Formation than the cementation.

1. Introduction

Reservoir quality is considered as the crucial factor for effective and viable tight sandstone oil exploration (Fic and Pedersen, 2013; Stroker et al., 2013; Liu et al., 2014; Xi et al., 2015a; Zhou et al., 2016). Tight sandstone reservoirs have generally experienced complicated diagenetic alterations, causing reservoirs to become tight progressively during burial and thermal evolution (Karim et al., 2010; Dutton and Loucks, 2010; Wolela, 2012; Yuan et al., 2015). To better predict reservoir quality due to diagenetic alteration, it is necessary to ascertain the nature of the diagenetic system and the processes involved. If

diagenetic reactions occurred in a closed geochemical system, the chemical reactions involved in diagenesis can be accurately constrained by mass balance equations, which provide a basis for making reservoir quality predictions using assumptions on primary mineral compositions related to facies and provenance (Bjørlykke and Jahren, 2012; Bjørlykke, 2014). Reservoir quality predictions, however, would be difficult to be made, when large-scale material exchanges occurred in an open geochemical system (Bjørlykke and Jahren, 2012). Therefore, the nature of the diagenetic system involved geochemically, whether it is a closed or an open system, must be understood when proposing a reasonable predictive model for sandstone reservoirs (Ajdukiewicz and

* Corresponding author.

E-mail address: xikelai@upc.edu.cn (K. Xi).<https://doi.org/10.1016/j.marpetgeo.2018.10.031>

Received 28 April 2018; Received in revised form 9 August 2018; Accepted 18 October 2018

Available online 21 October 2018

0264-8172/ © 2018 Elsevier Ltd. All rights reserved.

Lander, 2010; Yuan et al., 2015).

The issue relating to whether deeply buried diagenetic systems are open or closed has been under dispute over a long period. Some researchers insist that deeply buried diagenetic reactions mainly happen in a closed geochemical system where diagenetic alterations can be regarded as coupled dissolution-and-precipitation processes; and that the geochemical constraints for mass transfer during buried diagenetic reactions can be reasonably accepted (Giles and De Boer, 1990; Chuhan et al., 2001; Higgs et al., 2007; Bjørlykke and Jahren, 2012; Yuan et al., 2015). Other studies, however, showed that open geochemical system diagenesis also existed in some deeply buried sandstones where authigenic minerals can be externally sourced with byproducts being exported freely (Wilkinson et al., 1997; Taylor et al., 2010; Zhang et al., 2014; Worden et al., 2015). For example, ions can be transported from adjacent mudstones to reservoir sandstones and precipitate as the authigenic minerals (Wilkinson et al., 1997; Taylor et al., 2010; Zhang et al., 2014). Deep hydrothermal solution can also migrate to the reservoir sandstones through deep-fault and provide material sources for authigenic minerals (Worden et al., 2015; Xi et al., 2016).

The Upper Triassic Yanchang Formation is an important oil-bearing formation in the Ordos Basin. The sandstone reservoirs are tight and heterogeneous in this area (Zhou et al., 2016). Previously, the wide-range porosity variations were attributed to variations in the content of calcite cementation and chlorite coatings (Wang et al., 2017), suggesting that diagenesis is the primary control on reservoir quality. However, there has been little or no work done on whether the diagenetic system was an open or closed system. It is thus essential to understand the nature of the geochemical system involved in the diagenesis to better predict reservoir quality of the tight sandstone reservoirs. The main objectives of this research are: 1) to document sandstone diagenesis through detailed petrographic characterization and geochemical analysis, 2) to investigate the nature of the geochemical diagenesis system, 3) to discuss the paragenetic sequence of diagenesis and the impacts on reservoir quality in the Upper Triassic Yanchang Formation tight sandstones.

2. Geological background

The Ordos Basin is a polycyclic sedimentary craton basin located in the western part of the north China platform (Fig. 1). The basin is a gentle monocline with an east-to-west dip of less than 1° (Lai et al., 2016). It is bounded by the Qinling Mountains in the south, the Yin Mountains in the north, the Luliang Mountains in the east and the Helan-Liupan Mountains in the west with an area of about $250 \times 10^3 \text{ km}^2$ (Fig. 1). It can be further subdivided into 6 first-order sub-tectonic units, namely the Yimeng uplift and the Weibei uplift in the northern and southern margins, the Jinxi flexural fold belt and the Western edge thrusting belt in the eastern and western margins, the Tianhuan depression and the Shanbei slope in the central part of the basin (Fig. 1). The study area, as one of the most oil-rich zones in the Triassic reservoirs, is located in the southwestern part of the basin, encompassing the Jiyuan, Huanjiang and Longdong areas from north to south (Fig. 1).

During the Paleozoic-Mesozoic the Ordos Basin evolved from a Cambrian-Early Ordovician cratonic basin with divergent margins, through a Middle Ordovician-Middle Triassic cratonic basin with convergent margins to a Late Triassic-Early Cretaceous intraplate remnant cratonic basin (Yang et al., 2005). The structural framework of the basin was mainly developed during the Mesozoic (Tang et al., 2014), when a widespread Paleozoic marine to non-marine stratigraphic sequence was superimposed (Liu et al., 2008; Ritts et al., 2009). During the Middle to Late Triassic Period, the Ordos Basin changed from marine facies, through transitional facies to continental facies as a result of the Indo-China movement, developing into an inland lake basin (Ji et al., 2010). From the Middle Triassic to the Middle Jurassic the basin was predominantly filled with fluvial-lacustrine sediments (Zhao

et al., 2015). Two major Mesozoic petroleum systems are present in the basin namely, the Upper Triassic Yanchang Formation and Lower Jurassic Yan'an Formation (Duan, 2012).

The Upper Triassic Yanchang Formation sandwiched in-between the Middle Triassic Zhifang Formation and the Lower Jurassic Yan'an Formation (Fig. 2), comprises sediment sequences deposited from the Carnian to the Norian stages, which are dominated by alluvial fan, alluvial plain, deltaic, fluvial and lacustrine facies (Qiu et al., 2014). The provenances of the sediments are mainly derived from the Liupanshan and Qinling orogenic belts (Xie, 2016). The thickness of the Yanchang Formation ranges from about 200 m to 1400 m (Fig. 2), recording the evolution process of the formation, expansion, contraction, and extinction of a large lacustrine system (Zhu et al., 2013). The Yanchang Formation can be further divided into 10 members (Fig. 2), namely Chang 10 (Ch10) to Chang 1 (Ch1) from bottom to top of the formation (Duan et al., 2008). Among them, Chang 7 and Chang 4 + 5, developed at the most expansive stage of the palaeo Ordos Lake, are dominated by dark shales as excellent source rocks (Fig. 2). Chang 9 consists of thick shales and interbedded sandstones, acting as both source rocks and reservoirs. Other members consist predominantly of sandstones and siltstones with some interbedded mudstones (Tang et al., 2014). The studied members, Chang 8 and Chang 9, consist of thickly layered sandstones deposited in the braided-delta subaqueous distributary channels (Wang et al., 2017). In general, the Upper Triassic Yanchang Formation sandstone reservoirs are tight and heterogeneous (Zhou et al., 2016), with porosity ranging from 0.33 to 18.05% with an average of 8.27%, and the permeability varying from 0.001 to 56.32 mD with an average of 0.85 mD (Fig. 3).

3. Samples and methods

The studies focus on the Upper Triassic Yanchang Formation sandstones in the southwestern Ordos Basin where most of the producing oil fields are located and consequently most drillings have taken place. Over 500 core samples and 2713 reservoir porosity and permeability data were collected from the Research Institute of Petroleum Exploration and Development, Changqing Oilfield Company, PetroChina.

3.1. Thin section petrography and XRD mineralogy

More than 200 blue epoxy resin impregnated thin sections were prepared for petrographic and diagenesis analyses. The thin sections were partly stained by alizarin red for carbonate mineral determination. Point counting was performed on 34 tight sandstone samples. Each thin section was point counted with at least 400 points to obtain mineralogical compositions, authigenic minerals content, feldspar dissolution porosity data. Sorting of the sandstones were estimated and grain sizes for the samples were measured using a Zeiss Axioscope A1 APOL digital transmission microscope equipped with the Image-Pro Plus software.

A total of 96 reservoir sandstone samples were analyzed for whole-rock (bulk) and clay fraction ($< 2 \mu\text{m}$) mineralogy using X-Ray Diffraction (XRD). The sample preparation, analysis and interpretation procedures used by Moore and Reynolds (1997) and Hillier (2003) were adopted. About 5.0 g of each sample was crushed, milled in ethanol in a McCrone micronizing mill and then dried at 60 °C. Randomly oriented powders were prepared by top-loading into PMMA (Polymethylmethacrylate) sample holders designed with concentric circular geometry grooved shallow wells. The powder diffraction patterns were then collected using a D/MAX 2500 X-ray diffractometer with Cu K α radiation. All XRD data collected were firstly analyzed for phase identification using the search-match module of the Evaluation (EVA) software using the reference databases of the International Center for Diffraction Data (ICDD) Powder Diffraction File 2 (PDF-2) and Crystallography Open Database (COD). After phases were identified with EVA, they were further analyzed based on the Rietveld quantitative X-

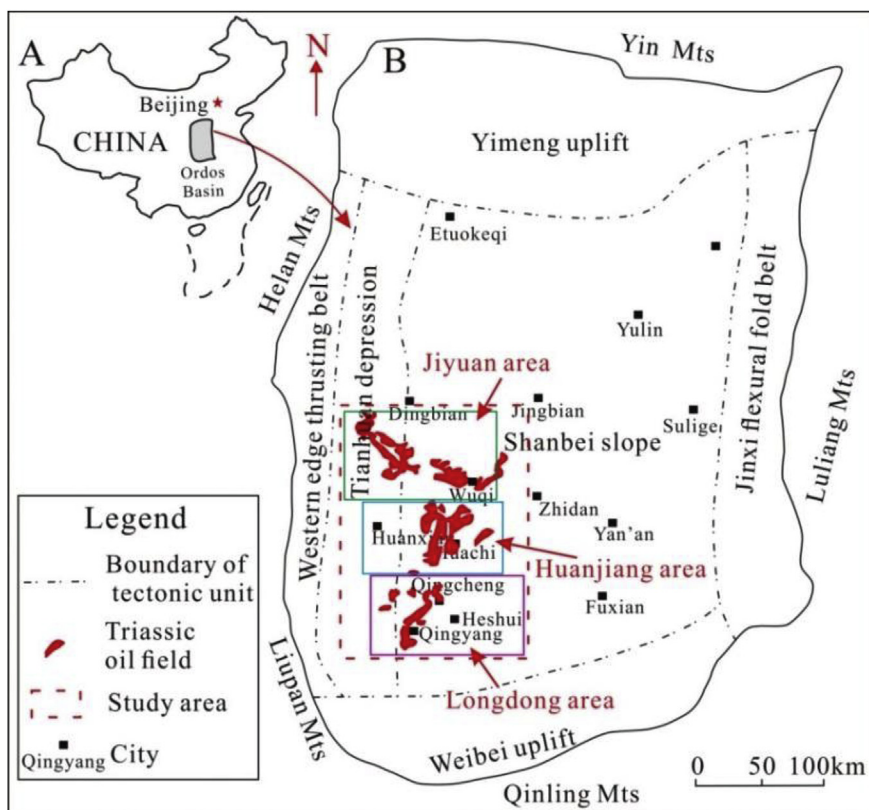


Fig. 1. Location map of the study area and sub-tectonic units of the Ordos Basin, (A) Location of the Ordos Basin; (B) Sub-tectonic units of the Ordos Basin and the study area (Modified from Zhou et al., 2016; Wang et al., 2017).

ray diffraction refinement approach.

3.2. Electron probe microanalysis (EPMA) and backscattered electron (BSE)

Electron probe microanalysis (EPMA) and backscattered electron (BSE) imaging were conducted for 17 samples by a JXA-8230 (JEOL) instrument at an accelerating voltage of 20 keV and a beam current of 10 nA. The beam size for EPMA on calcite varies from 3 to 10 μm according to the size and location of analyzed target. All the elements were calibrated using natural and synthetic standards including the following materials: SrO-celestite, Na_2O -albite, MgO-diopside, SiO_2 -diopside, K_2O -sanidine, CaO-diopside, TiO_2 -benitoite, FeO-hematite, MnO-bustamite, Cr_2O_3 -chromium oxide. Chemical analyses by EPMA yield values with an accuracy within about 1 wt% relative for major elements and 3 wt% relative for trace elements.

3.3. Scanning electron microscopy (SEM) and MAPS mineralogy

Based on petrographic analysis, twenty-three samples containing the major types of authigenic minerals and distinct pore spaces were analyzed using SEM equipped with an energy dispersive spectrometer (EDS). Thin section samples were gold-coated and observed under a Quanta FEG 450 at an accelerating voltage of 20 keV to identify the pore geometry, cement morphology, for the semi-quantitative estimation of mineral compositions and documenting the textural relationships between the minerals.

MAPS mineralogy, a micro-image splice technology based on BSE analysis, can make quantitative analysis of various mineral phases for each pixel by using FEI Helios 460 equipped with energy dispersive spectrometer (EDS). Thus, MAPS can provide high resolution BSE images and more accurate information for authigenic mineral structure and their paragenesis identification. MAPS mineralogy analysis was

performed on 5 samples. The samples were processed by argon ion milling, and then scanned under the EDS probe with an acceleration voltage of 3 keV and beam current of 0.4 nA. Scanning resolution was 20 nm. A total of 805 (23×35) BSE images were captured and automatically stitched together for each sample, forming a high-resolution image.

3.4. Cathodeluminescence (CL) petrograph

Cathodeluminescence (CL) images for 110 thicker polished thin sections were collected using a Cambridge CL8200 MK5 detector equipped on a Zeiss optical microscope with an acceleration voltage of 10 keV, a beam current of 250 μA and exposure durations of 10s (magnification $50 \times$), 30s (magnification $100 \times$) and 60s (magnification $200 \times$), respectively.

3.5. Fluid inclusion analysis

Seven core samples were prepared as double-polished thick sections of approximately 60–80 μm thickness for fluid inclusion petrographic analyses and microthermometric measurements. Microthermometry of fluid inclusions was conducted using a calibrated Linkam THMSG 600 heating and cooling stage which enables temperatures of phase transitions in the range of -180 $^{\circ}\text{C}$ to 500 $^{\circ}\text{C}$. Homogenization temperature (T_h) measurements were determined using a heating and cooling rate of 10 $^{\circ}\text{C}/\text{min}$ when the temperature was 0 – 60 $^{\circ}\text{C}$ or lower than -20 $^{\circ}\text{C}$, when the temperature were -20 – 0 $^{\circ}\text{C}$ or higher than 60 $^{\circ}\text{C}$, the heating, and cooling rate was changed to 5 $^{\circ}\text{C}/\text{min}$. Measurement precision was ± 1 $^{\circ}\text{C}$ for the homogenization temperature (T_h) and ± 0.1 $^{\circ}\text{C}$ for the final ice melting temperature, respectively.

In this study, thin section, CL, and fluid inclusion analyses were done in the Reservoir Geology and Basin Analysis Key Laboratory of China University of Petroleum. XRD, SEM-EDS and MAPS mineralogy

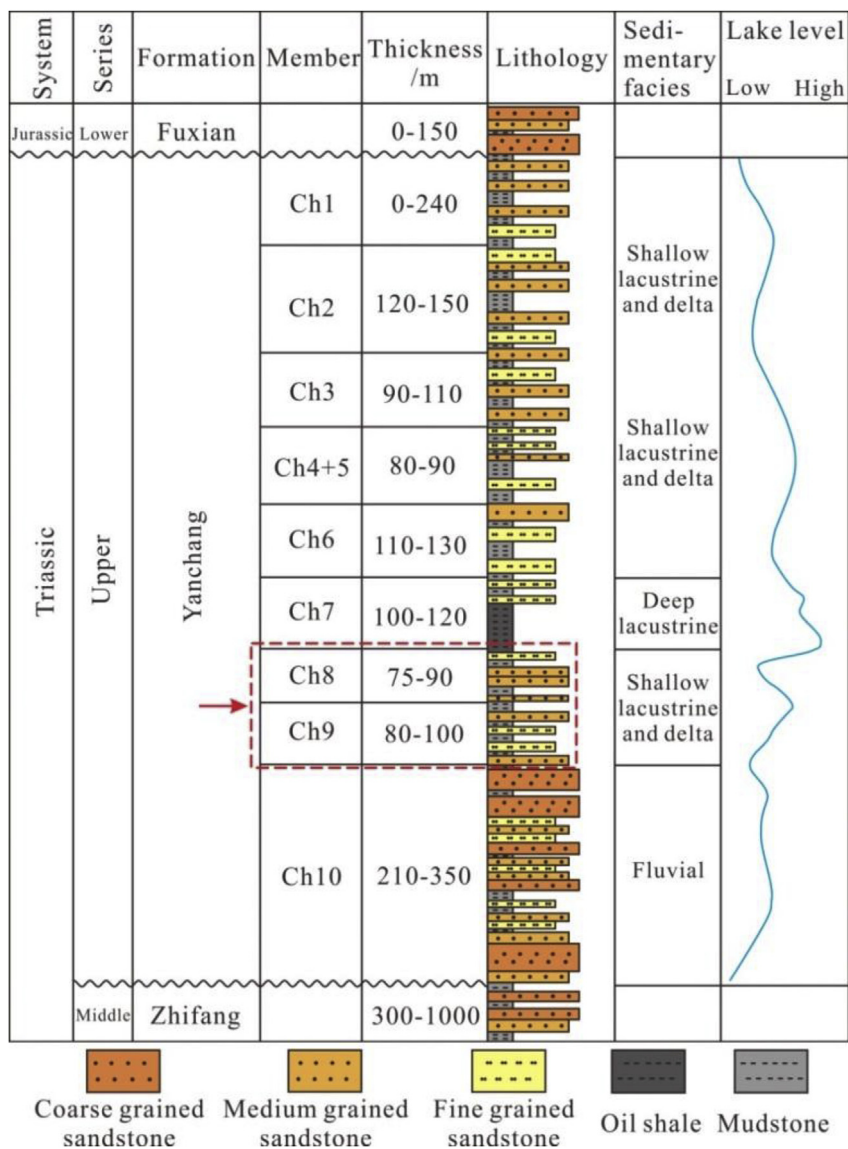


Fig. 2. Generalized Upper Triassic Yanchang Formation stratigraphy in the Ordos Basin (modified from Zhou et al., 2016).

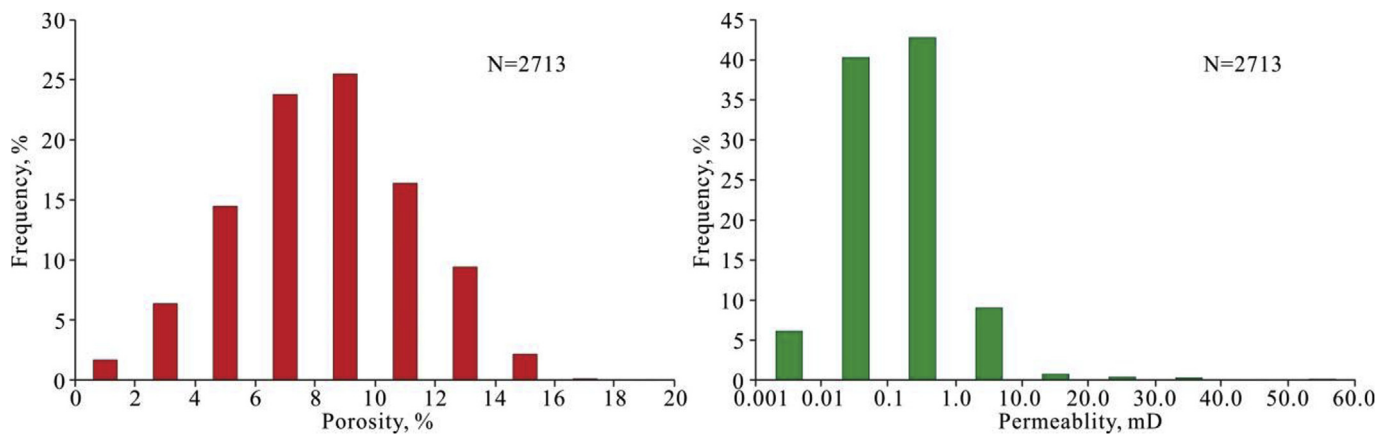


Fig. 3. Porosity and permeability distribution characteristics of the Upper Triassic Yanchang Formation tight sandstone reservoirs.

Table 1

Point counting results of rock composition, authigenic minerals content, feldspar dissolution porosity as well as sandstone grain size distribution, porosity and IGV in the Upper Triassic Yanchang Formation sandstones.

Well	Depth,m	Quartz, %	Feldspar, %	Rock fragment, %	Calcite cement, %	Quartz cement, %	Feldspar dissolution pores, %	Maximum grain size, μm	major grain size, μm	Porosity, %	IGV, %
Zh182	1912.8	32.22	43.33	24.44	2.5	2	1.1	0.6	0.20–0.40	13.51	23.07
Zh444	2160.33	23.60	42.70	33.71	1.4	–	0.2	0.4	0.12–0.35	10.15	28.65
Zh444	2168.47	29.05	37.99	32.96	2.5	–	0.9	0.6	0.20–0.50	11.48	26.90
Zh444	2191.52	31.87	34.07	34.07	6.5	1.5	0.9	0.5	0.10–0.30	8.4	24.50
Y465	2383.61	45.45	36.36	18.18	8.1	–	0.8	0.48	0.16–0.28	6.5	26.16
L98	2698.53	26.55	24.40	49.05	3.6	1.7	1.4	0.35	0.08–0.25	10.28	25.87
L98	2826.11	39.30	27.75	32.96	0.9	–	0.2	0.7	0.20–0.50	15.42	23.87
B436	2187	17.71	42.13	40.16	1.4	0.7	0.5	0.6	0.13–0.40	–	–
L220	2687.88	42.93	38.04	19.02	2.5	–	0.8	0.4	0.20–0.40	11.21	27.07
W70	1902.44	33.33	44.44	22.22	4.5	1	1.5	0.5	0.15–0.35	–	–
W70	1874.24	25.48	57.32	17.20	11.5	1.5	1.6	0.6	0.15–0.35	–	–
W70	1881.74	36.73	40.82	22.45	9.8	1.5	1.5	0.4	0.10–0.20	–	–
B12	1947.2	41.05	37.89	21.05	2.5	–	1	0.5	0.25–0.50	–	–
Y427	2425.75	30.11	56.99	12.90	1.4	0.5	0.5	0.7	0.25–0.60	13.58	25.02
B476	2181.9	25.85	32.72	41.44	4.5	–	1.2	0.6	0.15–0.40	9.02	27.65
B19	2027.6	37.78	40.00	22.22	8.1	–	1.1	0.6	0.25–0.50	8.29	24.67
B19	2048.14	41.05	37.89	21.05	6.4	2	1	0.5	0.25–0.50	5.91	26.71
B19	2043.32	36.84	35.79	27.37	4.5	3	1.2	0.5	0.20–0.50	5.6	28.07
B19	2033.24	36.17	36.17	27.66	6.4	3	1.5	0.5	0.20–0.50	9.21	22.91
B19	2027.6	37.78	40.00	22.22	8.1	–	1.1	0.6	0.25–0.50	9.45	23.51
W64	2188.5	24.16	53.93	21.91	2.5	1	1	0.3	0.12–0.25	12.93	24.55
G282	2589.15	26.76	27.68	45.56	1.4	0.8	1.1	0.5	0.15–0.35	–	–
B442	2358.2	33.88	47.54	18.58	2.5	0.5	0.1	0.5	0.2–0.4	14.72	22.36
X62	1966.15	24.18	52.20	23.63	1.4	–	0.6	0.6	0.14–0.50	13.27	25.93
X62	1967.15	24.00	51.43	24.57	4.5	–	0.7	0.5	0.15–0.50	13.26	22.91
X62	1973.35	24.85	29.23	45.92	9.5	1.7	1.1	0.45	0.13–0.30	6.39	23.51
M61	2586.7	27.81	42.78	29.41	1.4	0.5	0.6	0.5	0.20–0.40	–	–
M61	2600.1	24.73	41.94	33.33	3.6	0.5	0.6	0.5	0.20–0.45	–	–
L148	2368.44	36.78	41.95	21.26	8.1	–	1.8	0.4	0.14–0.30	9.4	24.26
Y441	2411.73	38.54	38.54	22.92	2.5	–	0.9	0.6	0.25–0.50	11.88	26.50
Y441	2470.82	27.27	57.75	14.97	1.4	–	0.3	0.4	0.20–0.40	11.98	26.92
Y441	2464.38	24.21	58.95	16.84	2.5	–	0.7	0.4	0.12–0.30	11.74	26.44
X127	1830.85	40.22	39.13	20.65	6.4	–	1.2	0.5	0.25–0.50	9.61	25.21
Zh22	1663.48	34.03	33.51	32.46	1.4	–	0.7	0.45	0.20–0.45	10.4	28.90

* Note: “–” means no data available.

were carried out at the Key Laboratory of Oil and Gas Reservoir of CNPC. EPMA and BSE analyses were performed at the Key Lab of Submarine Geosciences and Prospecting of Ocean University of China.

4. Results

4.1. Reservoir lithology

The detrital components in the tight sandstone of the Upper Triassic Yanchang Formation reservoirs comprise mainly quartz, feldspar and rock fragments. The sandstones are characterized by mostly fine to medium-grained (Table 1), moderate to well sorted and sub-angular to

sub-rounded detrital grains (Fig. 4A and B). Petrographic point counting reveals that detrital quartz ranges from 17.71 to 45.45% with an average of 31.83%, feldspar varies from 24.40 to 58.95% with an average of 41.28%, rock fragments range from 12.90 to 49.05% with an average of 26.89% (Table 1). The rock fragments were dominated by volcanic and low-grade metamorphic rock debris. The sandstones are texturally mature and compositionally immature with an average framework composition of Q₃₂F₄₁L₂₇, which are mainly classified as lithic arkoses with a small amount of arkose and feldspathic litharenite (Fig. 4C).

Bulk XRD data indicate that plagioclase is dominant with volumes four times that of K-feldspar in the studied tight sandstone reservoirs

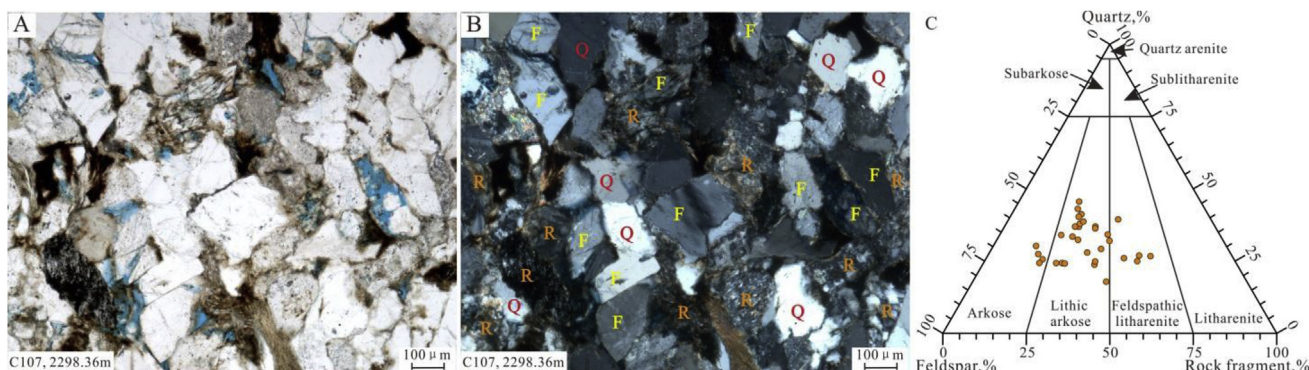


Fig. 4. Rock compositions of the Upper Triassic Yanchang Formation tight sandstone reservoirs: A and B, Photomicrograph showing textural and compositional features of the tight sandstones; C, Classification of sandstone using Folk's (1974) criteria; Q = quartz, F = feldspar, R = rock fragments.

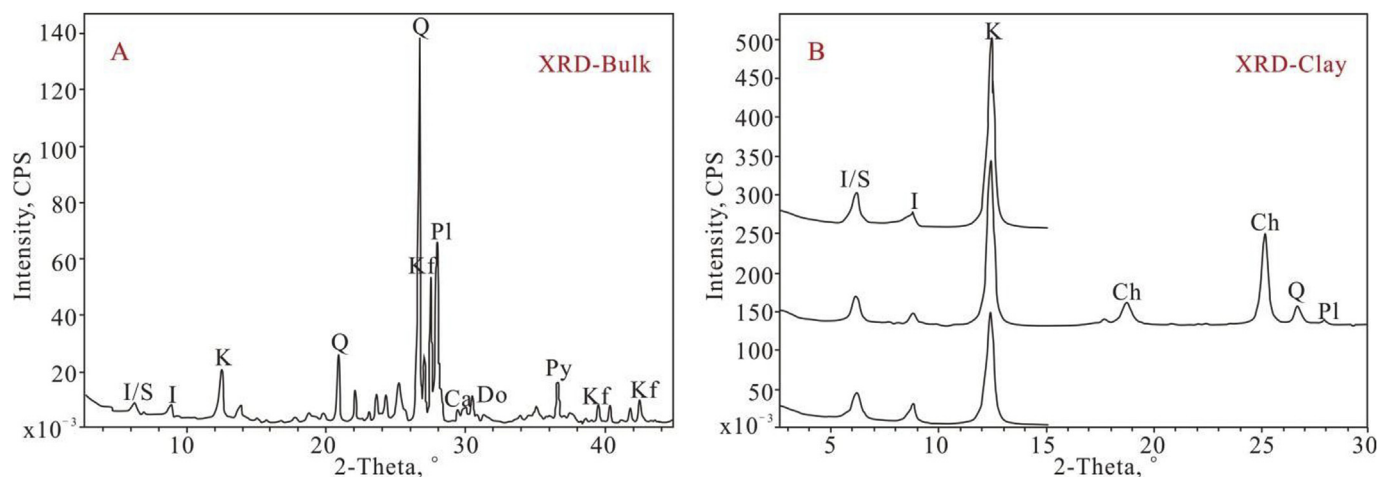


Fig. 5. Bulk and clay fraction XRD spectra of the tight sandstone reservoirs in the Upper Triassic Yanchang Formation; Q = quartz, Kf = K-feldspar, Pl = plagioclase, Ca = calcite, Do = dolomite, Py = pyrite, K = kaolinite, I = illite, I/S = illite/smectite, Ch = chlorite.

(Fig. 5A). Clay minerals mainly comprise kaolinite, mixed-layer illite/smectite (I/S), illite, and chlorite (Fig. 5B). Among them, chlorite is the most common one, and only small amounts of kaolinite, illite, and I/S are detected. Mixed-layer I/S is mainly of ordered interstratified with R = 3, namely illite percentages in mixed-layer I/S are higher than 85% (Lynch et al., 1997).

4.2. Diagenesis characteristics

4.2.1. Quartz cement

Quartz overgrowth is one of the most common authigenic minerals in the tight sandstone reservoirs studied (Zhou et al., 2016, Fig. 6A–F).

Generally, quartz overgrowths mainly develop in the sandstones where detrital quartz and volcanic rock fragments are abundant (Fig. 6A). Some quartz overgrowths are also associated with feldspar dissolution (Li et al., 2017, Fig. 6B). MAPS mineralogy images show that quartz overgrowths always occur in the micropores left by discontinuous chlorite coatings (Fig. 6C), indicating that only the continuous chlorite coatings with certain thickness can effectively inhibit quartz overgrowth. In some samples, two groups of quartz overgrowths can be seen on the cathodoluminescence (CL) images (Fig. 6D and E). The first generation (Qo-I) is characterized by dark, non-luminescence, whereas the second generation (Qo-II) exhibit a homogeneous brown luminescence color (Fig. 6D). The amount of Qo-I is higher than that of Qo-II in

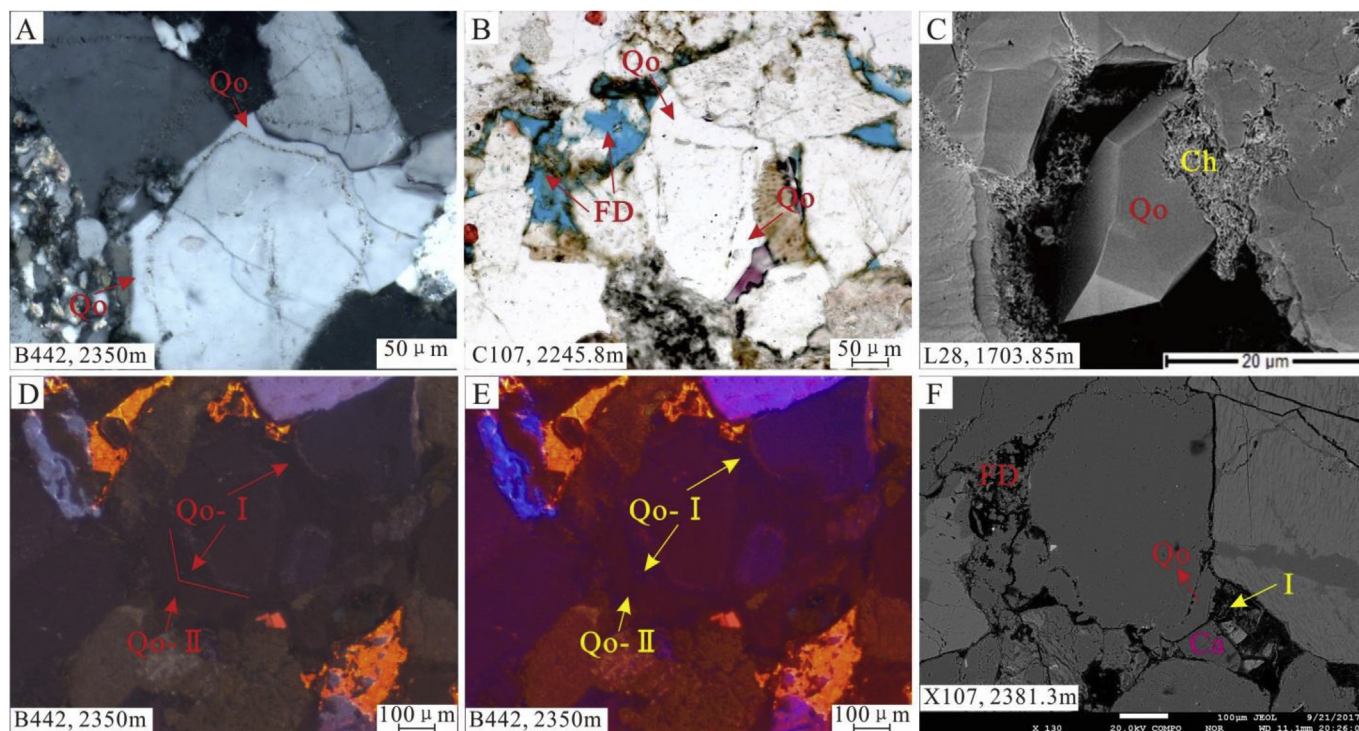


Fig. 6. Quartz cement characteristics of the Upper Triassic Yanchang Formation tight sandstone reservoirs: A, Photomicrograph of thin section showing quartz overgrowth; B, Photomicrograph of thin section showing quartz overgrowth and related feldspar dissolution; C, MAPS mineralogy image showing quartz overgrowth generated from the micro pores left by discontinuous chlorite coating; D, CL photomicrograph showing two generations of quartz overgrowth, dark non-luminescent (Qo-I) and brown luminescence color (Qo-II); E, idem with D to strengthen the CL color contrast of Qo-I and Qo-II; F, BSE image showing quartz overgrowth and related feldspar dissolution, calcite cement and illite. Qo-quartz overgrowth; Ch-chlorite coating; FD-feldspar dissolution; Ca-calcite cement; I-illite. (For interpretation of the references to color in this figure legend, the reader is referred to the Web version of this article.)

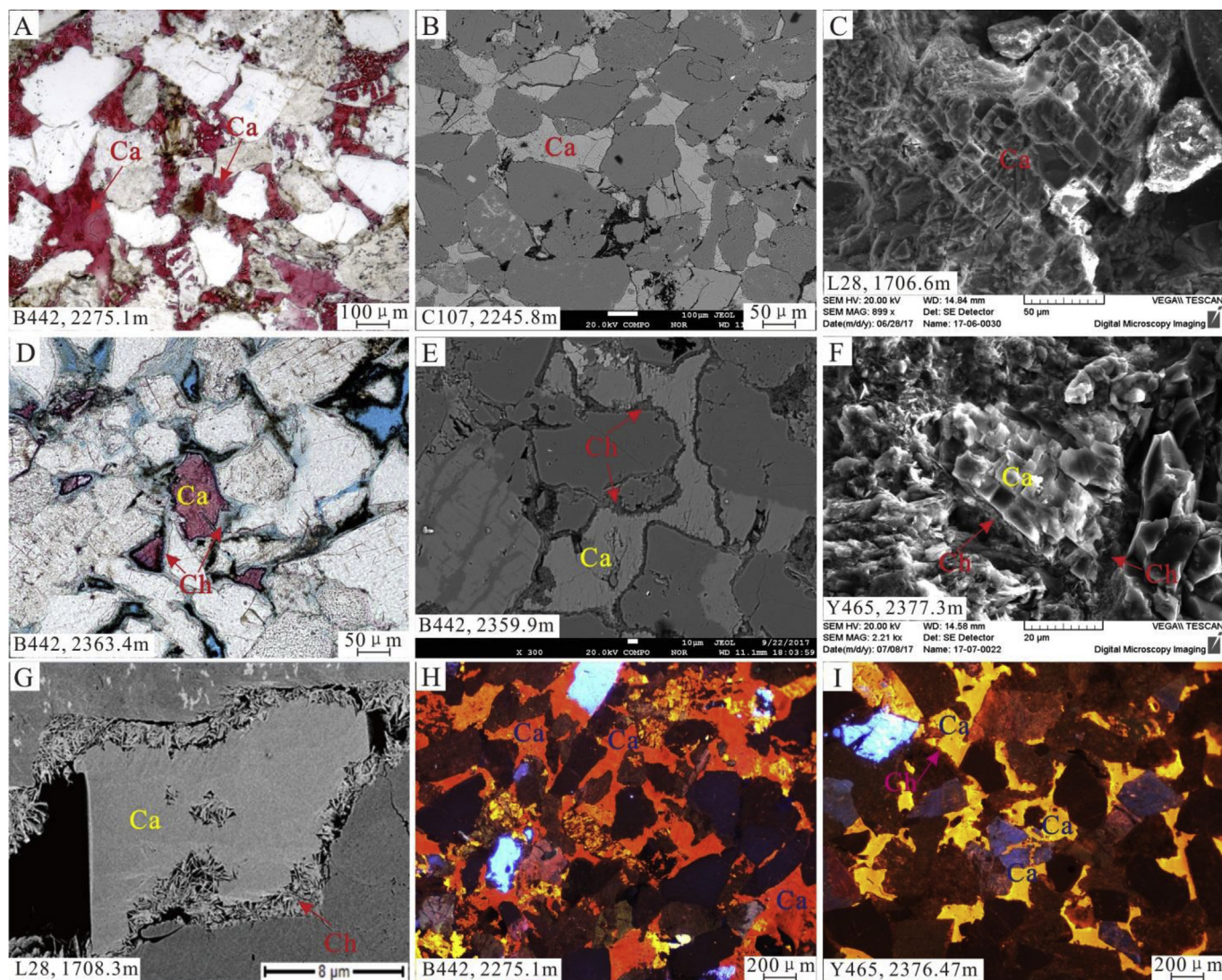


Fig. 7. Calcite cement characteristics in the Upper Triassic Yanchang Formation tight sandstone reservoirs: A, Photomicrograph of thin section showing calcite cement in close contact with detrital grains (Ca-I); B, Photomicrograph of BSE showing calcite cement in close contact with detrital grains (Ca-I); C, SEM image showing calcite cement in close contact with detrital grains (Ca-I); D, Photomicrograph of thin section showing calcite cement on top of chlorite coating (Ca-II); E, Photomicrograph of BSE showing calcite cement on top of chlorite coating (Ca-II); F, SEM image showing calcite cement on top of chlorite coating (Ca-II); G, MAPS mineralogy image showing calcite cement on top of chlorite with equal thickness (Ca-II); H, CL photomicrograph showing Ca-I with dull to reddish orange luminescence color; I, CL photomicrograph showing Ca-II with bright yellow luminescence color. Ca-calcite cement; Ch-chlorite coating. (For interpretation of the references to color in this figure legend, the reader is referred to the Web version of this article.)

the Upper Triassic Yanchang Formation sandstones. In addition, some quartz overgrowths are accompanied by feldspar dissolution, calcite cement and a small amount of fabric illite (Fig. 6B, F). The total content of quartz cement ranges from 0.5% to 3.0% with an average of 1.38% (Table 1).

4.2.2. Calcite cement and chlorite coating

Calcite cements, the volumetrically predominant cement type, occur as pore-filling blocky or mosaic aggregates in the Upper Triassic Yanchang Formation (Fig. 7A–G). Two types of calcite cements are present in the tight sandstone reservoirs studied. In some sandstones, calcite (Ca-I) was in close contact with detrital grains at places without chlorite coatings (Fig. 7A–C). The Ca-I calcite destroyed reservoir qualities seriously, resulting in fewer pore spaces being preserved. Another calcite type (Ca-II), however, precipitated on top of the chlorite coatings (Fig. 7D–G). Chlorite crystals grew perpendicular to the surface of the grains, and densely wrapped the detrital grains (Fig. 7D). The total content of calcite cements ranges from 0.9% to 11.5% with an

average of 4.3% (Table 1). Pore-lining chlorite coatings are of nearly equal thickness with 2–4 μm and mostly continuous (Fig. 7D, E, G). The chlorite coatings act as a distinct boundary between calcite and detrital grains, indicating that chlorite coating predate to Ca-II calcite cement (Fig. 7G). CL images show that the two types of calcite cements have different luminescence. Ca-I is characterized by dull to reddish orange luminescence color with a little yellow color mixture (Fig. 7H), whereas Ca-II mostly shows bright yellow luminescence color (Fig. 7I).

4.2.3. Feldspar dissolution

Plagioclase, the main type of feldspar in the studied reservoirs, commonly encountered partial intragranular dissolution in the Upper Triassic Yanchang Formation tight sandstone reservoirs (Fig. 8A–D). The porosity yielded from feldspar dissolution ranges from 0.1% to 1.8% with an average of 0.92% (Table 1). Plagioclase dissolutions are usually accompanied by calcite cements and minor amount of microcrystalline authigenic quartz (Fig. 8A–C). Some intragranular dissolution pores are completely or partly filled by calcite cements (Fig. 8D). K-

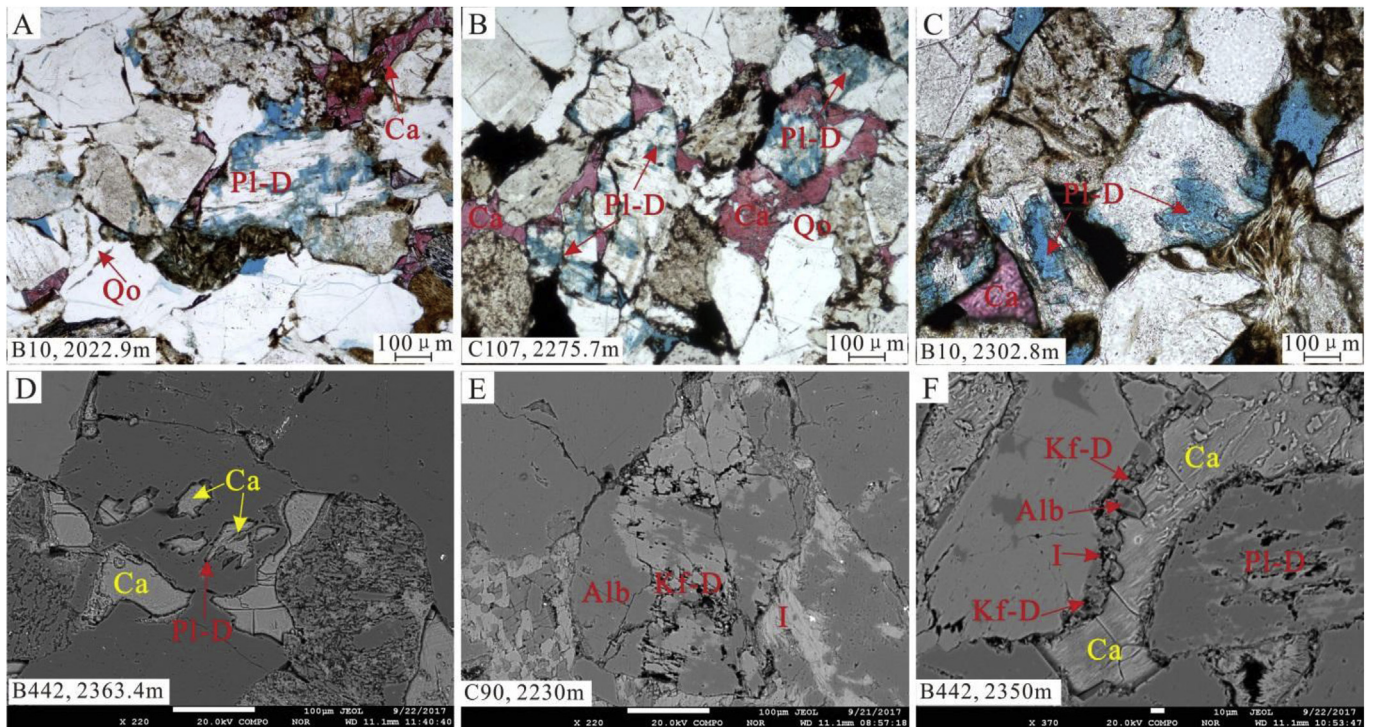


Fig. 8. Feldspar dissolution characteristics in the Upper Triassic Yanchang Formation tight sandstone reservoirs: A, B and C, Photomicrograph of thin section showing plagioclase dissolution with related calcite cement and quartz overgrowth; D, BSE image showing plagioclase dissolution with related calcite cement; E, Photomicrograph of BSE showing K-feldspar dissolution, albitization and related illite; F, BSE image showing plagioclase dissolution, K-feldspar dissolution and related calcite cement, euhedral albite, illite. Pl-D-plagioclase dissolution; Qo-quartz overgrowth; Ca-calcite cement; Kf-D-K-feldspar dissolution; Alb-albite; I-illite.

feldspar dissolution was texturally associated with albitization and illitization in the studied sandstones (Fig. 8E and F). The presence of euhedral albite between calcite cement and detrital grains (Fig. 8F) suggests that feldspar dissolution and albitization pre-dated calcite cementation.

4.3. Fluid inclusions in quartz cements

Aqueous inclusions commonly present in quartz overgrowths in the sandstones studied (Fig. 9A). Most of the aqueous inclusions consist of two phases, gas and liquid, at room temperature. The homogenization

temperatures (Th) of aqueous inclusions range from about 76.7 to 138.4 °C with an average of 105.64 °C, mainly centered around 90–130 °C (Table 2; Fig. 9B). The onset of quartz cementation was interpreted at about 70–80 °C, corresponding well with that observed in saline aquifers in the North Sea and the southern Songliao Basin, where the quartz overgrowth in the sandstone reservoirs mainly began to develop at about 80 °C and 70 °C, respectively (Bjørlykke and Egeberg, 1993; Xi et al., 2015b). Final ice melting temperatures (Tm) of the aqueous inclusions in the quartz cement ranges from –2.2 °C to –14.4 °C with an average of –7.0 °C, corresponding to the salinity between 3.71 and 18.13 NaCl wt.% equiv. with an average of 10.15

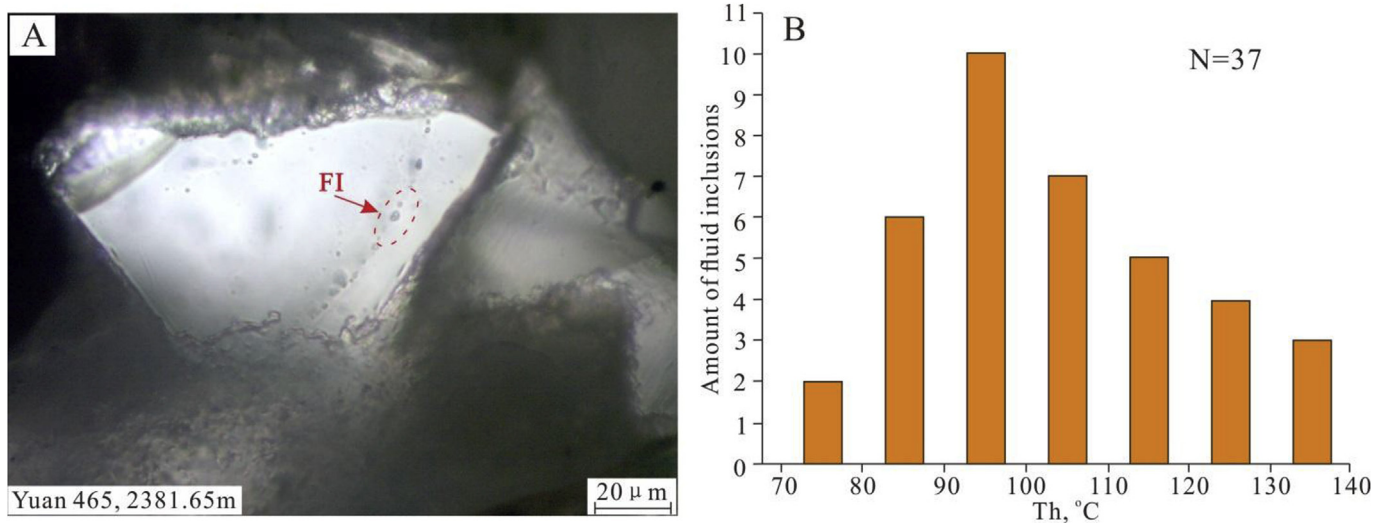


Fig. 9. Petrographic characteristics and homogenization temperature distribution of the Upper Triassic Yanchang Formation tight sandstone reservoirs: A, Photomicrographs of aqueous inclusions under transmitted light at the room temperature; B, Histogram of homogenization temperature (Th) for aqueous inclusions in quartz overgrowth. FI-fluid inclusion.

Table 2

Microthermometric data of the fluid inclusions in quartz overgrowth of the Upper Triassic Yanchang sandstone reservoirs, Th: homogenization temperatures; Tm, ice: final ice melting temperature.

Well	Depth, m	Th, °C	Tm, ice/°C	Salinity, NaCl wt.% equiv. (from Bodnar, 1993)
L28	1706.4	112.1	−10.5	14.46
L28	1706.4	119.2	−14.4	18.13
L28	1706.4	122.2	−13.1	16.99
L28	1706.4	105	−6.9	10.36
L28	1706.4	83.7	−9.3	13.18
L28	1706.4	108	–	–
L28	1706.4	104.1	–	–
L28	1706.4	98.3	–	–
L28	1706.4	103.9	−13.4	17.26
Y465	2832.08	90.3	−5.2	8.14
Y465	2832.08	92.1	−6.5	9.86
Y465	2832.08	93.8	–	–
Y465	2374.5	86.4	−2.2	3.71
Y465	2381.65	95.1	–	–
Y465	2381.65	97.2	−5.6	8.68
Y465	2381.65	78.4	−4.5	7.17
Y465	2381.65	108	−3.6	5.86
Y465	2381.65	86.6	–	–
Y465	2381.65	109.1	–	–
Y465	2381.65	138.4	–	–
Y465	2382.6	86.6	−6.3	9.6
Y465	2382.6	90	−7.1	10.61
Y465	2382.6	131.4	–	–
Y465	2382.6	127.8	–	–
L28	1698.73	90.1	−5.2	8.14
L28	1698.73	100.9	−4.9	7.73
L28	1698.73	90.5	−4.6	7.31
L28	1698.73	96.3	−2.3	3.87
L28	1698.73	115.8	−9.7	13.62
L28	1698.73	118.7	–	–
L28	1698.73	123.2	–	–
L28	1698.73	131.8	–	–
C107	2309.15	95.1	−6.6	9.98
C107	2309.15	89.3	−3.2	5.26
C107	2309.15	111.3	−10.1	14.40
C107	2309.15	121.1	–	–
C107	2309.15	76.7	−5.9	9.08

* Note: “–” means no data available.

NaCl wt.% equiv. (Table 2).

5. Discussion

5.1. Diagenetic minerals conversion and quartz cementation

Possible silica sources for quartz cement can be summarized as internal and external ones (Gluyas and Coleman, 1992; Thyne et al., 2001; Thyberg and Jahren, 2011; Xi et al., 2015b). Internal sources include biogenic silica, dissolution of unstable volcanic rock fragments and feldspar, clay mineral alteration and pressure solution of detrital grains, which mainly happened in a closed geochemical system (Bjørlykke and Egeberg, 1993; Kim and Lee, 2004; Peltonen et al., 2009; Hyodo et al., 2014; Xi et al., 2015b). For example, biogenic silica are the main sources for quartz overgrowth in the Gulf of Mexico sandstones (Land, 1997); quartz overgrowth in the Bohai Bay basin sandstones are mainly sourced from feldspar dissolution; clay mineral alteration and pressure solution of detrital grains act as the silica sources for quartz overgrowth in the Songliao Basin and the Dongjeom sandstones (Xi et al., 2015b; Kim and Lee, 2004). However, external sources can generally occur in open geochemical systems, such as from adjacent mudstones, deep fluid migration and so on (Gluyas and Coleman, 1992; Gluyas et al., 2000; Land and Milliken, 2000). For example, authigenic quartz in the Gulf Coast sandstones was mainly sourced from adjacent mudstones (Land and Milliken, 2000).

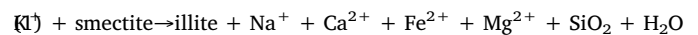
Firstly, biogenic silica is not a likely candidate for the origin of

quartz cement in the Upper Triassic Yanchang Formation since siliceous sponge spicules or other biogenic silica materials do not exist in the lacustrine facies (Zhao et al., 2015; Wang et al., 2017). The solubility of SiO₂ is quite low and is difficult to transport over long distances in geological systems without certain driving force (Bjørlykke and Jahren, 2012; Ronald and Edward, 1990). Thus, external sources for quartz cements should be mainly caused by some episodic events, such as episodic fluid flow from adjacent mudstones, deep fault fluids or deep hydrothermal solution (Ague, 1991; Boles et al., 2004). The homogenization temperature of the fluid inclusions in quartz cements showed a continuous distribution centered around 90–130 °C (Fig. 9), indicating that the associated diagenetic process was not disturbed by an episodic fluid flow enriched with silica materials distinctly (Bjørlykke and Jahren, 2012). Accordingly, quartz cements were probably sourced from internal mineral reactions in a closed geochemical system.

Element compositional characteristics are significantly different in the two groups of quartz overgrowth (Fig. 10A–D), suggesting that the main silica sources were changed in the different stages of quartz cementation. Compared to detrital quartz grains, the first generation of quartz overgrowth (Qo-I) is characterized by enrichment of MgO, Al₂O₃, and FeO associated with smectite to illite conversion (Fig. 10B, D; Hower et al., 1976; Hoffman and Hower, 1979; Boles and Franks, 1979). The second generation of quartz cement (Qo-II), however, is rich in Na₂O, K₂O, and Al₂O₃, closely associated with alteration or dissolution of feldspars (Fig. 10B, D; Bjørlykke and Jahren, 2012; Xi et al., 2015b; Yuan et al., 2015). These details are discussed as follows:

5.1.1. Quartz overgrowth via smectite to illite conversion

The Upper Triassic Yanchang Formation tight sandstones are rich in volcanic rock fragments (Fig. 4B). Volcanic rock fragments can be easily transformed into smectite during the early diagenesis stage (Campo et al., 2010; Shoval, 2004). During the burial process, unstable smectite will transform into mixed-layer I/S or discrete illite through the random mixed-layer I/S with increasing temperature (Bjørlykke, 2011), which can be expressed as (Boles and Franks, 1979):



Such a reaction mainly occurs at a temperature around 70 °C in sandstones (Hoffman and Hower, 1979; Peltonen et al., 2009; Thyberg et al., 2010; Metwally and Chesnokov, 2012), which coincides well with the onset temperature for quartz cementation (Table 2; Fig. 9B). Apart from quartz precipitation, some divalent ions, i.e. Ca²⁺, Fe²⁺, and Mg²⁺, will be released into pore waters as well. In addition, Al³⁺ is present extensively in the systems as a result of aluminosilicate mineral alteration. Among them, Ca²⁺ would be consumed by calcite cement precipitation quickly. Although Fe²⁺ and Mg²⁺ may be present in minor amounts, they would also be incorporated in the quartz cement. Therefore, the concentrations of Al₂O₃, FeO and MgO would be distinctly higher in the first generation of quartz overgrowth (Fig. 10B, D). Petrographic evidence of authigenic mineral paragenesis, such as quartz overgrowth coexists with illite mineralization and calcite cementation (Fig. 6F), also support the first generation of quartz cement was probably related to smectite to illite conversion.

5.1.2. Quartz overgrowth via feldspar dissolution

Smectite to illite conversion usually is quite rapid process in sandstones, which can only provide silica sources for quartz cementation around 70–100 °C (Gier et al., 2008; Peltonen et al., 2009). The homogenization temperature, however, shows a continuous process of quartz cementation up to 130 °C (Table 2; Fig. 9B). What is more, quartz overgrowth shows two distinct generations (Fig. 6E and F). There must be other silica sources available for the second generation of quartz cement in the Upper Triassic Yanchang Formation tight sandstone reservoirs. Petrographic evidence reveals that the second

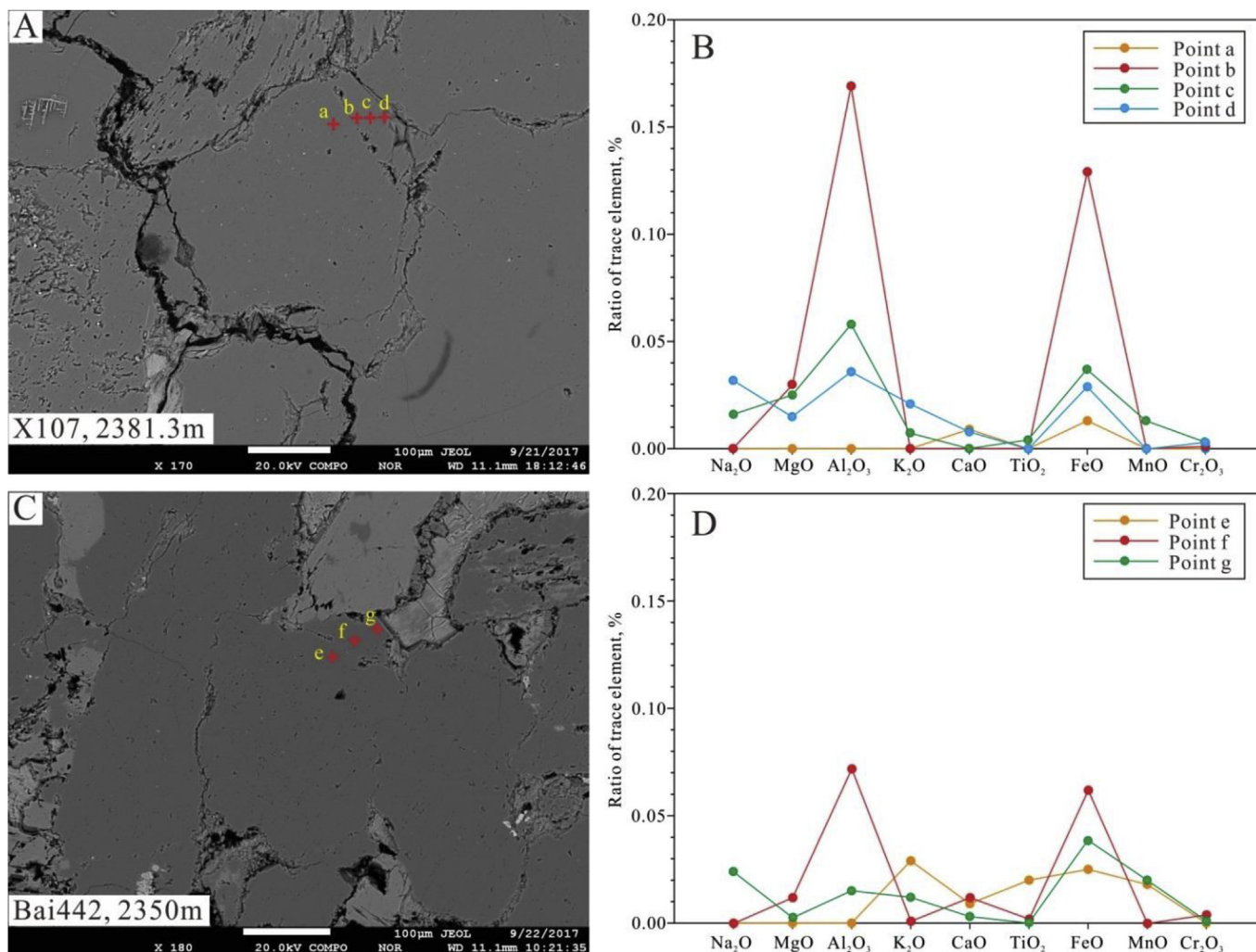


Fig. 10. In situ analysis of elemental compositions in two groups of quartz overgrowth: A and C, BSE images showing the EPMA analysis position in detrital quartz and quartz overgrowth; B and D, elemental composition distribution characteristics in two groups of quartz overgrowth. The results show that elemental composition distribution characteristics are significantly different in the two groups of quartz overgrowth. The first group of quartz cement is characterized by a higher amount of Al₂O₃, MgO, and FeO derived from smectite to illite conversion. The second group of quartz overgrowth, however, is abundant with Na₂O, K₂O with silica source provided by feldspar dissolution.

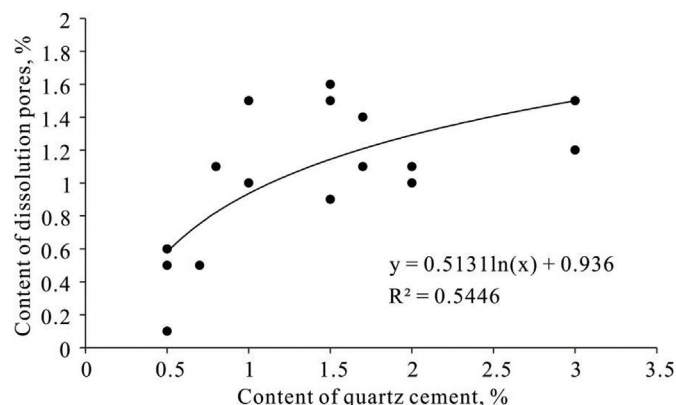
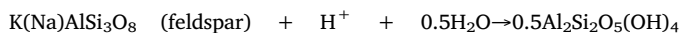


Fig. 11. Relationship between the amount of feldspar dissolution and quartz cement, showing a positive relationship.

generation of quartz cement was usually accompanied by feldspar dissolution (Fig. 6B, F), which may be a possible source for quartz cementation. The process of feldspar dissolution can be expressed as:



This reaction can generate aqueous silica and precipitate quartz cement locally (Bjørlykke and Jahren, 2012). The concentrations of K⁺ and Na⁺ in the pore water would increase with increasing amount of feldspar dissolution. These ions would be incorporated in quartz overgrowth, causing relatively higher amounts of Na₂O, K₂O. This is what has been measured by electron probe (Fig. 10B, D). There is also a positive relationship between the amount of feldspar dissolution pores and quartz cement (Table 1; Fig. 11). Therefore, feldspar dissolution most likely provided silica sources for the second group of quartz overgrowth in the Upper Triassic Yanchang Formation sandstone reservoirs.

It can be seen clearly that the elemental compositions in quartz overgrowth are sensitive to the silica sources. In the first group of quartz cementation, alteration of volcanic rock fragments and smectite to illite conversion provided more Al³⁺, Fe²⁺, and Mg²⁺, forming quartz cement with a higher amounts of Al₂O₃, MgO and FeO. Na₂O and K₂O formed from feldspar dissolution increased in the second group of quartz cement, although they are easiest transferable ions. Because MgO and FeO are absent from feldspar dissolution, their concentrations are decreased obviously in the second (late) generation of quartz cement. The elements unrelated to these two reactions showed

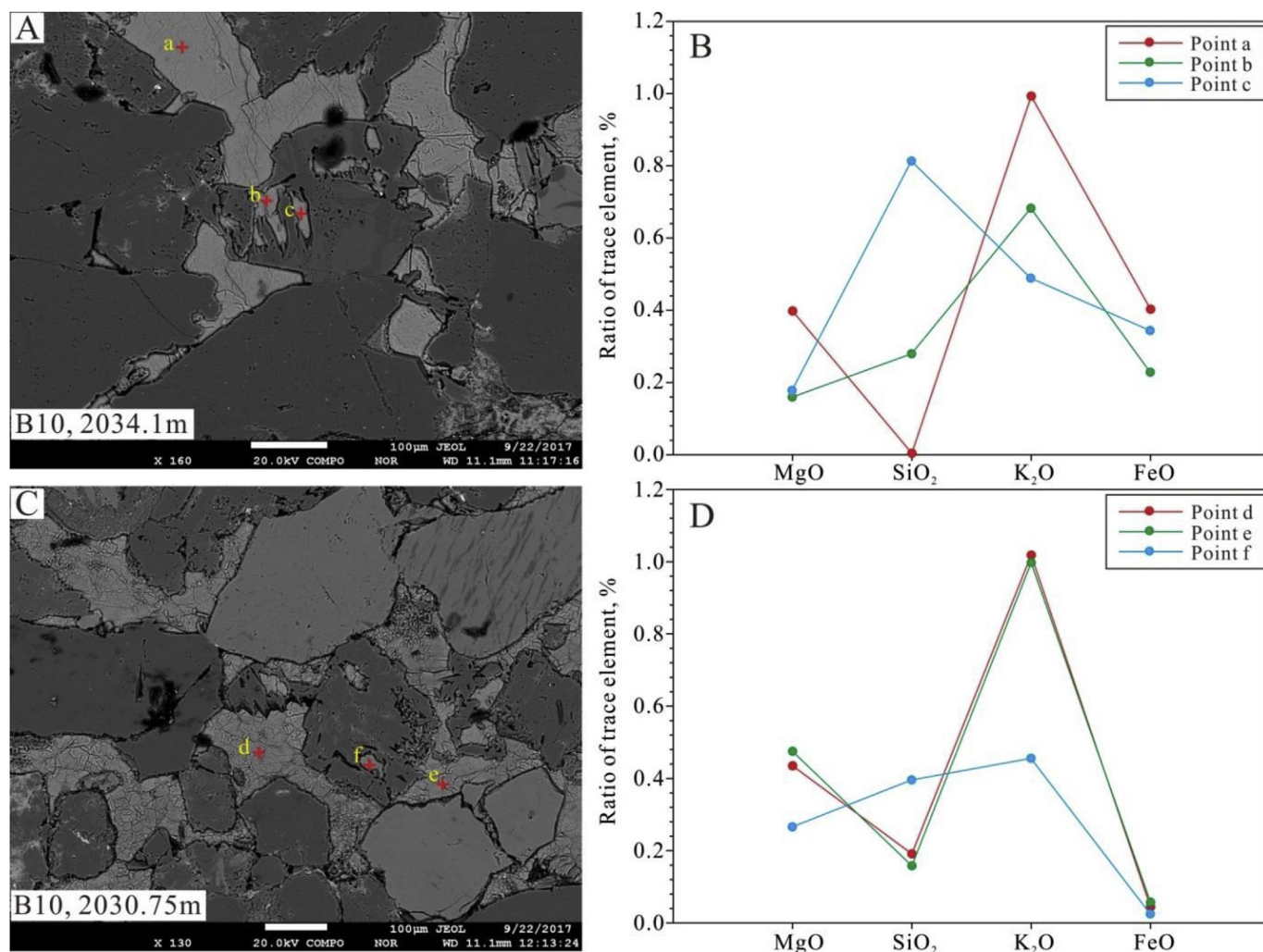
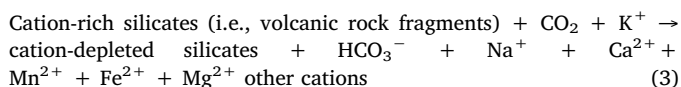


Fig. 12. In situ analysis of the elements in calcite cement precipitated in the primary intergranular pores and dissolved intragranular pores: A and C, BSE images showing the EPMA analysis positions in calcite cement; B and D, elemental distribution characteristics in calcite cement. The cations Mg^{2+} , Fe^{2+} , and K^+ altered from volcanic fragments are higher in the calcite cement of the primary intergranular pores and Si^{4+} is preserved more in the calcite within the dissolved intragranular pores, which provides evidence supporting a coupled dissolution-precipitation process occurred in the closed geochemical system.

insignificant differences between two groups of quartz cement (Fig. 10B, D). The salinity of the fluid inclusions in quartz cements increased with increasing homogenization temperature due to increasing cations of Al^{3+} , Fe^{2+} , and Mg^{2+} in the pore water (Table 1). All these suggest that diagenetic materials in the Upper Triassic Yanchang Formation tight sandstones are mainly sourced locally within the sandstone reservoir, with little or no external mass transportation involved. It thus can be concluded that quartz cementation mainly occurred in a closed geochemical system constrained by mass balance.

5.2. Silicates alteration and calcite cements precipitation

In order to precipitate the calcite cement, the divalent cation Ca^{2+} must be present in the pore water. The studied sandstones are characterized by abundant volcanic rock fragments and plagioclase (Fig. 4A and B). Firstly, with increasing temperature, organic matters decarboxylation in source rocks occurred and released CO_2 into the sandstone reservoirs, resulting in further alteration of the unstable volcanic rock fragments, which can be expressed as (Sample et al., 2017):



This reaction can provide abundant divalent cation Ca^{2+} accompanied by Mg^{2+} , Fe^{2+} and Mn^{2+} into reservoir pore water, which can then act as the major internal Ca^{2+} sources for the calcite cements. Plagioclase dissolution can also provide Ca^{2+} to calcite cementation. Plagioclase can be easily dissolved by CO_2 from organic matters decarboxylation in the sandstone reservoirs. Petrographic evidence showed that plagioclase dissolution pores were always accompanied by calcite cements in the Upper Triassic Yanchang Formation tight sandstones (Fig. 8A–D, F).

In a closed geochemical system, the cations Mg^{2+} , Fe^{2+} and K^+ altered from volcanic fragments can be easily incorporated into the calcite cement in the primary pores. These two cations, however, are difficult to migrate into the dissolved intragranular pores due to poor connectivity. Meanwhile, the byproduct of plagioclase dissolution, such as Si^{4+} and Al^{3+} , are difficult to be removed from plagioclase dissolution pores. The results of electron probe analyses show that the concentration of elemental compositions in calcite cement are significantly different in the primary intergranular pores and plagioclase dissolution pores (Fig. 12A–D). Calcite cements in the primary intergranular pores are enriched with MgO , FeO , and K_2O , while SiO_2 has a higher concentration in the calcite cements precipitated in the plagioclase dissolution pores (Fig. 12A–D). These differences on ion distribution further confirm the presence of a closed geochemical system

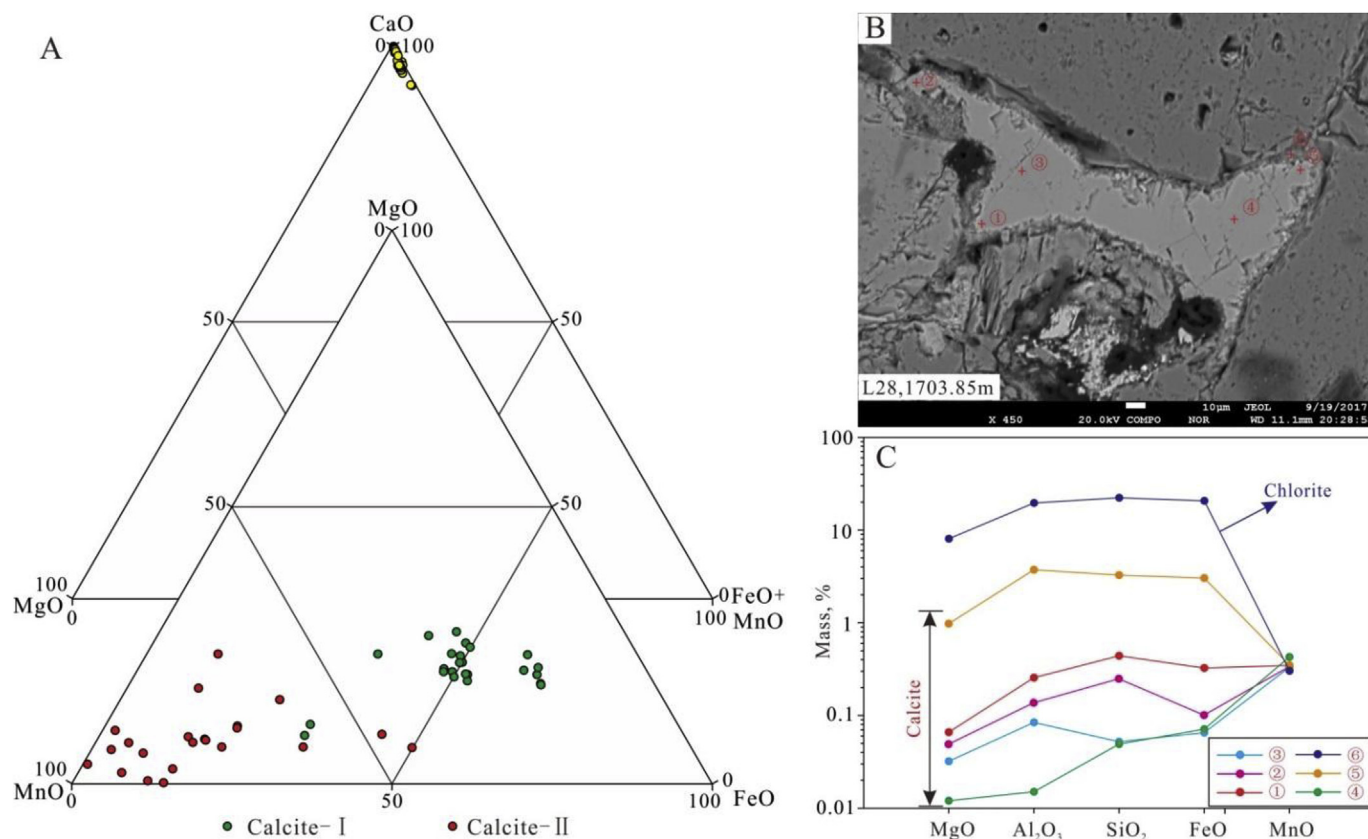


Fig. 13. In situ analysis of the elemental compositions in two types of calcite cement: A, Ternary diagrams showing normalized compositions of calcite cement from electron probe microanalysis in wt% oxides. B and C, BSE and EPMA results showing the heterogeneous distribution of elements in the calcite cement from the central part of the pore spaces to the edges of chlorite coatings. Both FeO and MgO are higher in Ca-I than Ca-II, indicating that the elements were generated and consumed in a closed geochemistry system.

in the Upper Triassic Yanchang Formation tight sandstone reservoirs.

The presence of relatively high K₂O concentration in the calcite cements indicated that potassium in the pore water was not disturbed by external sources (Fig. 12B, D), which is also indicative of a closed geochemical system (Jahren and Aagaard, 1992; Chuhan et al., 2001). In addition, minor amount of K-feldspar dissolution and albitization may have accelerated the smectite to illite conversion by providing enough K⁺ (Thyberg et al., 2010), and formed euhedral albite locally (Fig. 8E and F), which further supports a closed geochemical system in the studied sandstone reservoirs.

5.3. Interaction between calcite cement and chlorite coatings

The Ca-II calcites appear to be always associated with chlorite coatings in the Upper Triassic Yanchang Formation tight sandstone reservoirs. Electron probe analysis indicates that the concentration of Fe²⁺ and Mg²⁺ are significantly different in the two types of calcite cement (Ca-I and Ca-II). Both FeO and MgO are enriched in Ca-I than Ca-II calcite cements (Fig. 13A). The concentrations of Fe²⁺ and Mg²⁺ in pore water would be increased through the alteration of volcanic rock fragments at the early stage of diagenesis (Sample et al., 2017). On one hand, these ions can provide sources for ferromagnesian minerals, i.e., chlorite, in some pore spaces. On the other hand, they may be incorporated in authigenic minerals as associated elements. Petrographic evidence revealed that Ca-II precipitated later than chlorite coatings in the Upper Triassic Yanchang Formation sandstone reservoirs (Fig. 7D–G). Therefore, Fe²⁺ and Mg²⁺ in the pore water would be firstly consumed by the formation of chlorite coating in the associated pore spaces. As a result, the pore water would be lack of Fe²⁺ and Mg²⁺ when the Ca-II calcite began to precipitate. There was no chlorite

coating formation in the pores where Ca-I calcite precipitation in the Upper Triassic Yanchang Formation sandstones. The ions Fe²⁺ and Mg²⁺ were probably preserved in the pore water and were incorporated in the Ca-I calcite cement. The higher amount of FeO in the Ca-I calcite results in a high FeO/MnO ratio, which explains the dull-reddish orange luminescence color (Fig. 7H). On the contrary, the Ca-II calcite cement showed bright yellow luminescence color (Fig. 6I) due to a low FeO/MnO ratio (Scholle and Ulmer-Scholle, 2003; Omer et al., 2014).

In situ element analyses by EMPA indicated that Mg²⁺, Fe²⁺, Al³⁺ and Si⁴⁺ concentrations in the calcite cements were all lower at the central part of the pores than around the chlorite coatings, whereas Mn²⁺ was distributed homogeneous everywhere (Fig. 13B and C). This is because the cations of Mg²⁺, Fe²⁺, Al³⁺, and Si⁴⁺ are closely related to chlorite coatings but Mn²⁺ is not directly associated with chlorite. During the formation of chlorite coatings, these cations would be gathered from center to edge of the pores. The concentration of Mn²⁺ was not influenced by chlorite coatings. All these suggest that the concentrations of FeO and MgO are strictly constrained by interactions between calcite cements and chlorite coatings. In other words, these ions were formed and consumed in a closed geochemical system where diagenetic fluids were not significantly disturbed by external materials.

5.4. Paragenetic sequence of diagenesis and the impacts on reservoir quality

The paragenetic sequence of diagenesis for the Upper Triassic Yanchang Formation is reconstructed and illustrated in Fig. 14 by synthesizing the petrographic evidence, mineral reactions associated with cement sources, interactions between authigenic minerals, and the formation temperature of major cements.

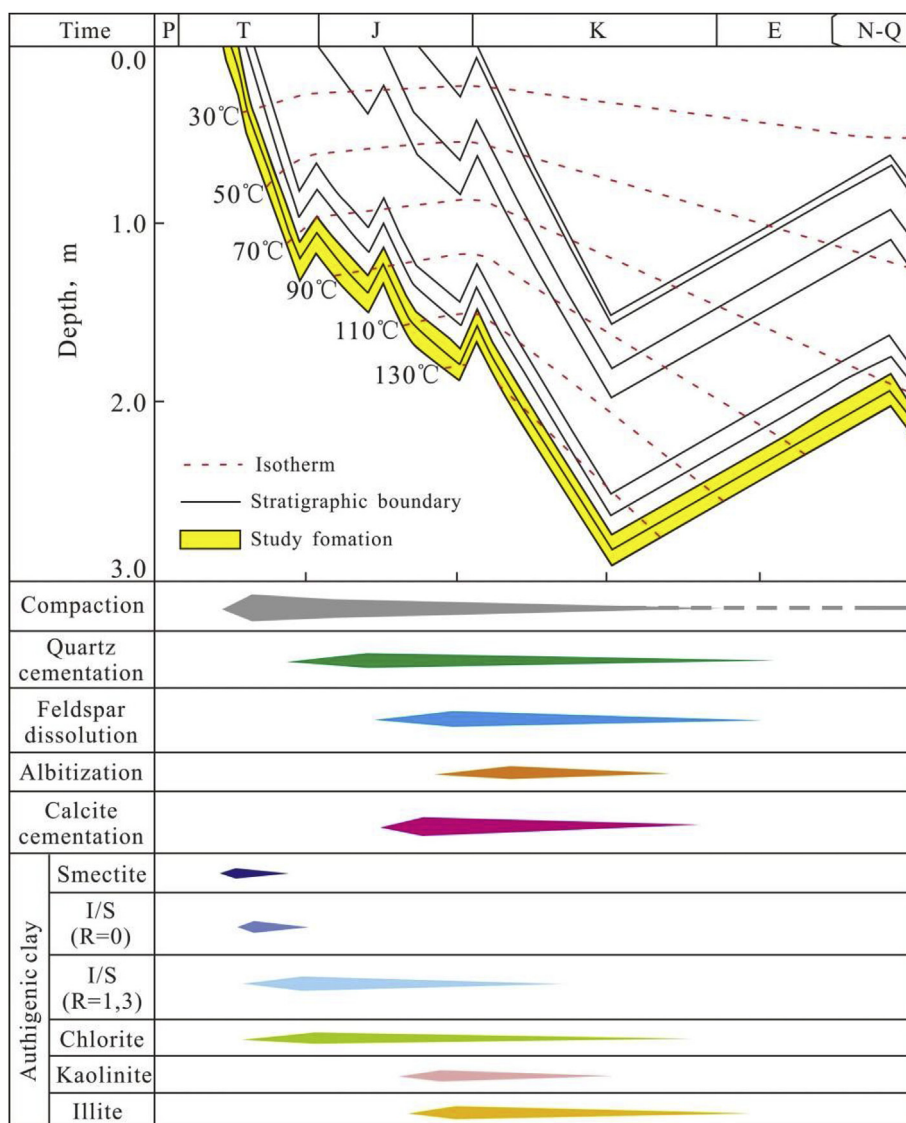


Fig. 14. Burial, thermal and diagenetic history a of the Upper Triassic Yanchang Formation tight sandstone reservoirs.

Reservoir quality is primarily a function of provenance, sedimentary textures and diagenesis (Xi et al., 2015a). In the studied reservoirs, the sandstones have the same provenance, and the grain size and sorting are similar among the samples (Table 1), probably having insignificant effects on reservoir quality. Thus, the reservoir quality is mainly controlled by diagenesis. Compaction, starting immediately after deposition, can be evaluated by the intergranular volume (IGV). The intergranular volume (IGV) found in the studied samples from the petrographic analysis show little depth dependence with values between about 22.36% and 28.90% with an average of 25.74% (Table 1). Cementation also played a major role in reducing porosity and permeability in the studied sandstone reservoirs. The total content of cements ranges from 0.9% to 13.0% with an average of 5.0% (Table 1). However, feldspar dissolution is only limited in the Upper Triassic Yanchang Formation tight sandstones, varying from 0.1% to 1.8% with an average of 0.92% (Table 1). A plot of intergranular volume (IGV) versus cement volume indicates that mechanical compaction has played a more important role than cementation in destroying the primary porosity of the Upper Triassic Yanchang Formation (Fig. 15). Compaction has accounted for about 27.8%–44.1% with an average of 36.3% of the total intergranular pore volume loss during the burial process, assuming an initial porosity is 40% (Houseknecht, 1987; Lundegard, 1992).

6. Conclusions

- (1) There are two groups of quartz cement in the Upper Triassic Yanchang Formation tight sandstone reservoirs. The first group was formed early during the conversion from smectite to illite, whereas the second group occurred late with feldspar dissolution providing the silica source.
- (2) Two types of calcite cement are present in the tight sandstone reservoirs. The Ca-I calcite cement developed early and is rich in Fe^{2+} and Mg^{2+} , whereas the Ca-II calcite cement developed after and over the chlorite coatings contains with little or no Fe^{2+} and Mg^{2+} . Dissolution of volcanic rock fragments and plagioclase provided the Ca^{2+} sources for the calcite cements. K-feldspar dissolution and albitization formed euhedral albite locally.
- (3) Elemental compositions in the diagenetic minerals are strictly constrained by involved authigenic minerals interactions, suggesting a closed geochemical system where diagenesis alterations occurred in accordance with the general principle of mass balance.

Acknowledgments

This study is co-funded by National Natural Science Foundation of China (KX: 41702141, YC: U1762217), the National Postdoctoral

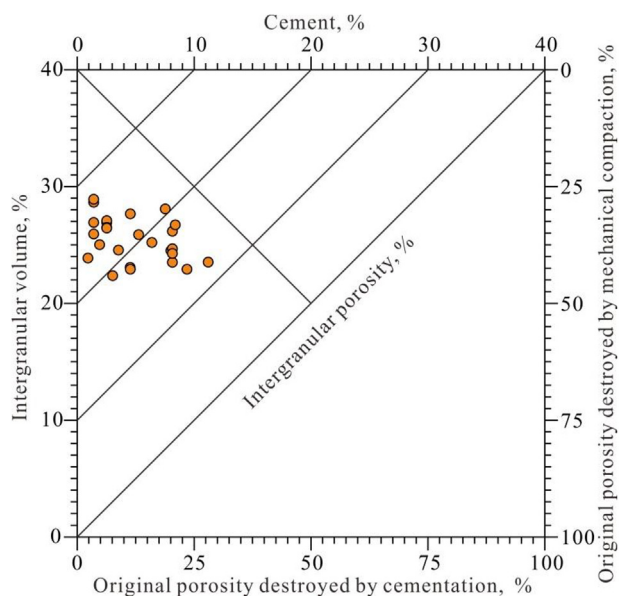


Fig. 15. Plot of intergranular volume (IGV) versus volume of cement in the Upper Triassic Yanchang Formation sandstone reservoirs (modified from Houseknecht, 1987 and Lundegard, 1992), showing that the reservoir quality is controlled more by compaction than cementation.

Program for Innovative Talents (KX: BX201600154), the National Major Project on Innovative characterization techniques and development models for low-permeability and tight oil reservoirs (KL: 2017ZX05009001), the Natural Science Foundation of Shandong Province (KX: ZR2017BD005), the China Postdoctoral Science Foundation Project (KX: 2016M600568), the Postdoctoral Innovative Foundation Project of Shandong Province (KX: 201702023) the Fundamental Research Funds for the Central Universities (YC: 15CX08001A) and Key Project of CNPC (KX: 2016B-03). We are also grateful to the Changqing Oilfield Company, PetroChina for providing their in-house database and permission to publish.

References

Ague, J.J., 1991. Evidence for major mass transfer and volume strain during regional metamorphism of pelites. *Geology* 19, 855–858.

Ajdukiewicz, J.M., Lander, R.H., 2010. Sandstone reservoir quality prediction. The state of the art. *AAPG (Am. Assoc. Pet. Geol.) Bull.* 94, 1083–1091.

Bjørlykke, K., 2011. Open-system chemical behavior of Wilcox Group mudstones. How is large-scale mass transfer at great burial depth in sedimentary basins possible? A discussion. *Mar. Petrol. Geol.* 28, 1381–1382.

Bjørlykke, K., 2014. Relationships between depositional environments, burial history, and rock properties. Some principal aspects of diagenetic process in sedimentary basins. *Sediment. Geol.* 301, 1–14.

Bjørlykke, K., Egeberg, P.K., 1993. Quartz cementation in sedimentary basins. *AAPG (Am. Assoc. Pet. Geol.) Bull.* 77, 1538–1548.

Bjørlykke, K., Jahren, J., 2012. Open or closed geochemical systems during diagenesis in sedimentary basins: constraints on mass transfer during diagenesis and the prediction of porosity in sandstone and carbonate reservoirs. *AAPG (Am. Assoc. Pet. Geol.) Bull.* 96, 2193–2214.

Bodnar, R.J., 1993. Revised equation and table for determining the freezing point depression of H₂O-NaCl solutions. *Geochem. Cosmochim. Acta* 57, 683–684.

Boles, J.R., Eichhubl, P., Garven, G., Chen, J., 2004. Evolution of a hydrocarbon migration pathway along basin-bounding faults: evidence from fault cement. *AAPG (Am. Assoc. Pet. Geol.) Bull.* 88, 947–970.

Boles, J.R., Franks, S.G., 1979. Clay diagenesis in Wilcox sandstones of Southwest Texas: implications of smectite diagenesis on sandstone cementation. *J. Sediment. Res.* 49, 55–70.

Campo, D.M., Papa, D.C., Nieto, F., Hongn, F., Petrinovic, I., 2010. Integrated analysis for constraining palaeoclimatic and volcanic influences on clay-mineral assemblages in orogenic basins (Palaeogene Andean foreland, Northwestern Argentina). *Sediment. Geol.* 228, 98–122.

Chuhan, F.A., Bjørlykke, K., Lowrey, C.J., 2001. Closed system burial diagenesis in reservoir sandstones: examples from the Garn Formation at Haltenbanken area, offshore mid-Norway. *J. Sediment. Res.* 71, 15–26.

Duan, Y., 2012. Geochemical characteristics of crude oil in fluvial deposits from Maling oilfield of Ordos Basin, China. *Org. Geochem.* 52, 35–43.

Duan, Y., Wang, C., Zheng, C., Wu, B., Zheng, G., 2008. Geochemical study of crude oils from the Xifeng oilfield of the Ordos Basin, China. *J. Asian Earth Sci.* 31, 341–356.

Dutton, P.S., Loucks, G.R., 2010. Diagenetic controls on the evolution of porosity and permeability in lower Tertiary Wilcox sandstones from shallow to ultradeep (200–6700 m) burial, Gulf of Mexico Basin, U.S.A. *Mar. Petrol. Geol.* 27, 69–81.

Fic, J., Pedersen, K.P., 2013. Reservoir characterization of a “tight” oil reservoir, the middle Jurassic Upper Shaunavon Member in the Whitemud and Eastbrook pools, SW Saskatchewan. *Mar. Petrol. Geol.* 44, 41–59.

Folk, R.L., 1974. *Petrology of Sedimentary Rocks*. Hemphill, Austin, Texas, pp. 182.

Gier, S., Worden, H.R., Johns, D.W., Kurzweil, H., 2008. Diagenesis and reservoir quality of Miocene sandstones in the Vienna Austria. *Mar. Petrol. Geol.* 25, 681–695.

Giles, M.R., De Boer, R.B., 1990. Origin and significance of redistribution secondary porosity. *Mar. Petrol. Geol.* 7, 378–397.

Gluyas, J., Coleman, M., 1992. Material flux and porosity changes during sediment diagenesis. *Nature* 356, 52–54.

Gluyas, J., Garland, C., Oxtoby, N.H., Hogg, J.C., 2000. Quartz cement: The Miller’s tale. In: Worden, R.H., Morad, S. (Eds.), *Quartz Cementation in Sandstones*, vol. 29. International Association of Sedimentologists Special Publication, pp. 199–218.

Higgs, K.E., Zwingmann, H., Reyes, A.G., Funnell, R.H., 2007. Diagenesis, porosity evolution, and petroleum emplacement in tight gas reservoirs, Taranaki Basin, New Zealand. *J. Sediment. Res.* 77, 1003–1025.

Hillier, S., 2003. Quantitative analysis of clay and other minerals in sandstones by X-ray powder diffraction (XRPD). In: Worden, R., Morad, S. (Eds.), *Clay Mineral Cements in Sandstones*. International Association of Sedimentologist, Special Publication, Oxford, International, pp. 213–251.

Hoffman, J., Hower, J., 1979. Clay mineral assemblages as low-grade metamorphic geothermometers: application to the thrust-faulted disturbed belt of Montana, USA. In: *Aspects of Diagenesis*. Society for Sedimentary Geology, Special Publication, pp. 55–79.

Houseknecht, W.D., 1987. Assessing the Relative Importance of Compaction Processes and Cementation to Reduction of Porosity in sandstones. *AAPG (Am. Assoc. Pet. Geol.) Bull.* 71, 633–642.

Hyodo, A., Kozdon, R., Pollington, D.A., Valley, W.J., 2014. Evolution of quartz cementation and burial history of the Eau Claire formation based on in situ oxygen isotope analysis of quartz overgrowths. *Chem. Geol.* 384, 168–180.

Hower, J., Eslinger, E., Hower, M.E., Perry, E.A., 1976. Mechanism of burial metamorphism of argillaceous sediment: 1. Mineralogical and chemical evidence. *Geol. Soc. Am. Bull.* 87, 725–737.

Jahren, J.S., Aagaard, P., 1992. Diagenetic illite-chlorite assemblages in arenites: Part 1. Chemical evolution. *Clay Clay Miner.* 40, 540–546.

Ji, L., Yan, K., Meng, F., Zhao, M., 2010. The oleaginous Botryococcus from the Triassic Yanchang Formation in Ordos Basin, Northwestern China: morphology and its paleoenvironmental significance. *J. Asian Earth Sci.* 38, 175–185.

Karim, A., Piper, P.G., Piper, J.M.D., 2010. Controls on diagenesis of Lower Cretaceous reservoir sandstones in the western Sable Subbasin, offshore Nova Scotia. *Sediment. Geol.* 224, 65–83.

Kim, Y., Lee, Y., 2004. Origin of quartz cement in the lower Ordovician Dongjeom formation, Korea. *J. Asian Earth Sci.* 24, 327–335.

Lai, J., Wang, G.W., Ran, Y., Zhou, Z.L., Cui, Y.F., 2016. Impact of diagenesis on the reservoir quality of tight oil sandstones: the case of Upper Triassic Yanchang Formation Chang 7 oil layers in Ordos Basin, China. *J. Petrol. Sci. Eng.* 145, 54–65.

Land, L.S., 1997. Mass transfer during burial diagenesis in the Gulf of Mexico sedimentary basin: An overview. In: Montañez, I.P., Gregg, J.M., Shelton, K.L. (Eds.), *Basinwide Diagenetic Patterns: Integrated Petrologic, Geochemical and Hydrologic Considerations*, vol. 57. SEPM Special Publication, pp. 29–39.

Land, L.S., Milliken, K.L., 2000. Regional loss of SiO₂ and CaCO₃, and gain of K₂O during burial diagenesis of Gulf Coast mudrocks, U.S.A. In: Worden, R.H., Morad, S. (Eds.), *Quartz Cementation in Sandstones*, vol. 29. International Association of Sedimentologists Special Publication, pp. 183–197.

Li, Z., Wu, S., Xia, D., Zhang, X., Huang, M., 2017. Diagenetic alterations and reservoir heterogeneity within the depositional facies: A case study from distributary-channel belt sandstone of Upper Triassic Yanchang Formation reservoirs (Ordos Basin, China). *Mar. Petrol. Geol.* 86, 950–971.

Liu, C., Zhao, H., Zhao, J., Wang, J., Zhang, D., Yang, M., 2008. Temporospatial coordinates of the evolution of the Ordos basin and its mineralization responses. *Acta Geol. Sin.* 82, 1229–1243.

Liu, M., Liu, Z., Liu, J., Zhu, W., Huang, Y., Yao, X., 2014. Coupling relationship between sandstone reservoir densification and hydrocarbon accumulation: a case from the Yanchang Formation of the Xifeng and Ansai areas, Ordos Basin. *Petrol. Explor. Dev.* 41, 185–192.

Lundegard, P., 1992. Sandstone porosity loss - a “big picture” view of the importance of compaction. *Journal of Sedimentary Petrology* 62, 250–260.

Lynch, L.F., Mack, E.L., Land, S.L., 1997. Burial diagenesis of illite/smectite in shales and the origins of authigenic quartz and secondary porosity in sandstones. *Geochem. Cosmochim. Acta* 61, 1995–2006.

Metwally, M.Y., Chesnokov, M.E., 2012. Clay mineral transformation as a major source for authigenic quartz in thermo-mature gas shale. *Appl. Clay Sci.* 55, 138–150.

Moore, D.M., Reynolds, R.C., 1997. *X-ray Diffraction and the Identification and Analysis of Clay Minerals*. Oxford University Press, Oxford.

Omer, M.F., Omer, D., Zebari, B.G., 2014. High-resolution cathodoluminescence spectroscopy of carbonate cementation in Khurmala Formation (Paleocene–Eocene) from Iraqi Kurdistan Region, Northern Iraq. *J. Afr. Earth Sci.* 100, 243–258.

Peltonen, C., Marcussen, Ø., Bjørlykke, K., Jahren, J., 2009. Clay mineral diagenesis and quartz cementation in mudstones: the effects of smectite to illite reaction on rock properties. *Mar. Petrol. Geol.* 26, 887–898.

Qiu, X., Liu, C., Mao, G., Deng, Y., Wang, F., Wang, J., 2014. Late Triassic tuff intervals in

- the Ordos basin, Central China: their depositional, petrographic, geochemical characteristics and regional implications. *J. Asian Earth Sci.* 80, 48–160.
- Ritts, B.D., Weislogel, A., Graham, S.A., Darby, B.J., 2009. Mesozoic tectonics and sedimentation of the giant polyphase nonmarine intraplate Ordos Basin, Western North China block. *Int. Geol. Rev.* 51, 95–115.
- Ronald, K.S., Edward, D.P., 1990. Secondary porosity revisited: the chemistry of feldspar dissolution by carboxylic acids and anions. *AAPG (Am. Assoc. Pet. Geol.) Bull.* 74, 1795–1808.
- Sample, J.C., Torres, M.E., Fisher, A., Hong, W., Destgrigneville, C., Defliese, W.F., Tripathi, A., 2017. Geochemical constraints on the temperature and timing of carbonate formation and lithification in the Nankai Trough, NanTroSEIZE transect. *Geochem. Cosmochim. Acta* 198, 92–114.
- Scholle, P.A., Ulmer-Scholle, D.S., 2003. A Color Guide to the Petrography of Carbonate Rocks, vol. 77. American Association of Petroleum Geologists Memoir, pp. 474.
- Shoval, S., 2004. Deposition of volcanogenic smectite along the southeastern NeoTethys margin during the oceanic convergence stage. *Appl. Clay Sci.* 24, 299–311.
- Stroker, M.T., Harris, B.N., Elliott, C.W., Wampler, M.J., 2013. Diagenesis of a tight gas sand reservoir: Upper Cretaceous Mesaverde Group, Piceance Basin, Colorado. *Mar. Petrol. Geol.* 40, 48–68.
- Tang, X., Zhang, J., Wang, X., Yu, B., Ding, W., Xiong, J., Yang, Y., Wang, L., Yang, C., 2014. Shale characteristics in the southeastern Ordos Basin, China: implications for hydrocarbon accumulation conditions and the potential of continental shales. *Int. J. Coal Geol.* 128–129, 32–46.
- Thyberg, B., Jahren, J., 2011. Quartz cementation in mudstones: Sheet-like quartz cement from clay-mineral to 1000 °C. *Comput. Geosci.* 18, 899–947.
- Thyberg, B., Jahren, J., Winje, T., Bjørlykke, K., Faleidel, J., Marcussen, Ø., 2010. Quartz cementation in late Cretaceous mudstones, northern North Sea: changes in rock properties due to the dissolution of smectite and precipitation of micro-quartz crystals. *Mar. Petrol. Geol.* 27, 1752–1764.
- Thyne, G., Boudreau, B.P., Ramm, M., Midtbo, R.E., 2001. Simulation of potassium feldspar dissolution and illitization in the Statfjord Formation, North Sea. *AAPG (Am. Assoc. Pet. Geol.) Bull.* 85, 621–635.
- Taylor, T.R., Giles, M.R., Hathon, L.A., Diggs, T.N., Braunsdorf, N.R., Birbiglia, G.V., 2010. Sandstone diagenesis and reservoir quality prediction: models, myths, and reality. *AAPG (Am. Assoc. Pet. Geol.) Bull.* 94, 1093–1132.
- Wang, G., Chang, X., Yin, W., Li, Y., Song, T., 2017. Impact of diagenesis on reservoir quality and heterogeneity of the Upper Triassic Chang 8 tight oil sandstones in the Zhenjing area, Ordos Basin, China. *Mar. Petrol. Geol.* 83, 84–96.
- Wilkinson, M., Darby, D., Haszeldine, R.S., Couples, G.D., 1997. Secondary porosity generation during deep burial associated with overpressure leak-off: Fulmar Formation, United Kingdom Central Graben. *AAPG (Am. Assoc. Pet. Geol.) Bull.* 81, 803–813.
- Wolela, A., 2012. Diagenetic evolution and reservoir potential of the Barremian-Cenomanian Debre Libanose Sandstone, Blue Nile (Abay) Basin, Ethiopia. *Cretac. Res.* 36, 83–95.
- Worden, R.H., Benshatwan, M.S., Potts, G.J., Elgarmadi, S.M., 2015. Basin-scale Fluid Movement Patterns Revealed by Veins: Wessex Basin. *Geofluids*, UK, pp. 1–26.
- Xi, K., Cao, Y., Jahren, J., Zhu, R., Bjørlykke, K., Haile, B.G., Zheng, L., Hellevang, H., 2015a. Diagenesis and reservoir quality of the lower cretaceous Quantou formation tight sandstones in the southern songliao basin, China. *Sediment. Geol.* 330, 90–107.
- Xi, K., Cao, Y., Jahren, J., Zhu, R., Bjørlykke, K., Zhang, X., Cai, L., Hellevang, H., 2015b. Quartz cement and its origin in tight sandstone reservoirs of the Cretaceous Quantou formation in the southern Songliao basin, China. *Mar. Petrol. Geol.* 66, 748–753.
- Xi, K., Cao, Y., Zhu, R., Haile, B.G., Zheng, L., Hellevang, H., 2016. Evidences of localized CO₂-induced diagenesis in the Cretaceous Quantou Formation, southern Songliao Basin, China. *International Journal of Greenhouse Gas Control* 52, 155–174.
- Xie, X., 2016. Provenance and sediment dispersal of the Triassic Yanchang Formation, southwest Ordos Basin, China, and its implications. *Sediment. Geol.* 335, 1–16.
- Yang, Y., Li, W., Ma, L., 2005. Tectonic and stratigraphic controls of hydrocarbon systems in the Ordos basin: a multicycle cratonic basin in central China. *AAPG (Am. Assoc. Pet. Geol.) Bull.* 89, 255–269.
- Yuan, G.H., Cao, Y., Gluyas, J., Li, X., Xi, K., Wang, Y., Jia, Z., Sun, P., Oxtoby, N.H., 2015. Feldspar dissolution, authigenic clays, and quartz cements in open and closed sandstone geochemical systems during diagenesis: typical examples from two sags in Bohai Bay Basin, East China. *AAPG (Am. Assoc. Pet. Geol.) Bull.* 99, 2121–2154.
- Zhang, Q., Zhu, X., Steel, R.J., Zhong, D., 2014. Variation and mechanisms of clastic reservoir quality in the Paleogene Shahejie Formation of the Dongying Sag, Bohai Bay Basin, China. *Petrol. Sci.* 11, 200–210.
- Zhao, J., Mountney, N.P., Liu, C., Qu, H., Lin, J., 2015. Outcrop architecture of a fluvio-lacustrine succession: Upper Triassic Yanchang Formation, Ordos Basin China. *Mar. Petrol. Geol.* 68, 394–413.
- Zhou, Y., Ji, Y., Xu, L., Che, S., Niu, X., Wan, L., Zhou, Y., Li, Z., You, Y., 2016. Controls on reservoir heterogeneity of tight sand oil reservoirs in Upper Triassic Yanchang Formation in Longdong Area, southwest Ordos Basin, China: Implications for reservoir quality prediction and oil accumulation. *Mar. Petrol. Geol.* 78, 110–135.
- Zhu, X., Deng, X., Liu, Z., Sun, B., Liao, J., Hui, X., 2013. Sedimentary characteristics and model of the shallow braided delta in large-scale lacustrine: an example from Triassic Yanchang Formation in Ordos Basin. *Earth Sci. Front.* 20, 19–28.